International
Progress Report

IPR-05-19

Äspö Hard Rock Laboratory

Äspö Pillar Stability Experiment

Thermo-mechanical 3D back analyze of the heating phase

Billy Fälth
Ola Kristensson
Harald Hökmark

Clay Technology AB

August 2005

Svensk Kärnbränslehantering AB
Swedish Nuclear Fuel
and Waste Management Co
Box 5864
SE-102 40 Stockholm Sweden
Tel 08-459 84 00
+46 8 459 84 00
Fax 08-661 57 19
+46 8 661 57 19

Äspö Hard Rock
Laboratory

Report no.	No.
IPR-05-19	F86K
Author	Date
Billy Fälth Ola Kristensson Harald Hökmark	August 2005
Checked by	Date
J. Christer Andersson Derek Martin	2005-08-29
Approved	Date
Anders Sjöland	2005-11-04

Äspö Hard Rock Laboratory

Äspö Pillar Stability Experiment

Thermo-mechanical 3D back analyze of the heating phase

Billy Fälth
Ola Kristensson
Harald Hökmark

Clay Technology AB

August 2005

Keywords: Thermal conductivity, Thermal expansion, Insulation, Stress, Temperature, Sensitivity analysis, Code Bright, Heater, Back calculation, Displacement, Young's modulus, Finite element, FEM

Abstract

This report concerns thermo-mechanical simulations of the Äspö Pillar Stability Experiment (APSE). The two main purposes in this work have been to:

- Back-calculate a temperature field that agrees with measured values in the experiment.
- Calculate the thermal stresses in the pillar.

Data of the experiment geometry and of rock mechanical properties were used as input to a fully 3-dimensional Code_Bright finite element continuum model. The continuum was assumed to be linearly elastic. Heat transport was approximated to take place by linear heat conduction only. Temperatures measured at the walls of the two deposition holes were used as thermal boundary conditions, while temperatures measured at the side of the pillar were used to calibrate the rock heat conductivity. Similarly, the heat loss across different sections of the tunnel floor was calibrated to match data given for the temperature between insulation and floor. At the right side of the experiment, the input power was adjusted to account for heat loss caused by water movements and boiling.

The simulated temperature field matches the measured temperatures well in the pillar region, i.e. close to the holes and the heaters. In the rock volume surrounding the pillar region the temperatures are somewhat over predicted.

A sensitivity analysis was conducted in order to evaluate the effects on the stress of over-predicting the temperatures in the surrounding rock. The excess temperature increase in the surrounding rock was compensated for by decreasing the thermal expansion coefficient in this region by a corresponding factor. When doing so, the stress component normal to the tunnel direction in the pillar, i.e. the tangential stress, decreased by 10 %.

Also, the sensitivity, in terms of the tangential stress dependence on the magnitude of Young's modulus in the surrounding rock, was investigated. When the Young's modulus was decreased from 76 GPa to 55 GPa in the surrounding rock, the tangential stress in the pillar was reduced by 15 %.

In the model believed to be the most realistic one, using the lower values of thermal expansion coefficient and Young's modulus, the tangential stress in the pillar 0.02 m from the wall of the open hole at 2 – 4 m depth, was found to be approximately 20 MPa at day 38 (before the power increase) and 30 MPa at day 52 (after the power increase).

Sammanfattning

Denna rapport behandlar termomekanisk simulering av Äspö Pelar Stabilitet Experiment (APSE). De två huvudsyftena i detta arbete har varit att:

- Med hjälp av beräkningar återskapa ett temperaturfält som överensstämmer med uppmätta värden i experimentet.

- Beräkna de termiska spänningarna i pelaren.

Givna data på experimentgeometrin och på bergets mekaniska egenskaper användes som indata till en fullt 3-dimentionell Code_Bright finita element kontinuumsmodell. Kontinuumet antogs vara linjärelastiskt. Värmetransport approximerades till att ske endast genom linjär värmeledning. Temperaturerna uppmätta på väggarna i de två deponeringshålen användes som termiska randvillkor, medan temperaturer uppmätta vid sidan av pelaren användes för att kalibrera bergets värmekonduktivitet. På liknande sätt var värmeförlusten i olika sektioner av tunneln kalibrerad till att passa uppmätt temperatur mellan isolering och golv. På höger sida av experimentet justerades effekten för att ta hänsyn till värmeförluster orsakade av vattenrörelser och kokning.

Det simulerade temperaturfältet överensstämmer bra med de uppmätta temperaturerna i pelarregionen, d.v.s. nära hålen och värmarna. I bergvolymen som omger pelarregionen är temperaturerna något överpredikterade.

En känslighetsanalys utfördes för att utvärdera vilken effekt de överpredikterade temperaturerna i det omgivande berget har på spänningen. Den överdrivna temperaturökningen i det omgivande berget kompenserades genom att minska den termiska expansionskoefficienten i denna region med en motsvarande faktor. Genom detta minskade spänningskomponenten vinkelrät mot tunnelriktningen, dvs. den tangentiella spänningen i pelaren, med 10 %.

Den tangentiella spänningens beroende på elasticitetsmodulen i det omgivande berget, har också undersökts. När elasticitetsmodulen minskades från 76 GPa till 55 GPa i det omgivande berget reducerades den tangentiella spänningen med 15 %.

I den modell som anses vara mest realistisk, där de lägre värdena på den termiska expansionskoefficienten och elasticitetsmodulen används, erhölls tangentiella spänningar i pelaren, 0.02 m från väggen i det öppna hålet vid 2 – 4 m djup, på ungefär 20 MPa dag 38 (före effektökningen) och 30 MPa dag 52 (efter effektökningen).

Contents

1 Introduction

The Äspö Pillar Stability Experiment (APSE) specifically addresses the problem of spalling in the walls of deposition holes /Andersson, 2003, 2005/. A tunnel with a rounded floor was excavated by use of careful blasting technique in sparsely fractured rock. The rounded floor and the excavation technique together gave high tangential stresses in the floor region. A full-scale deposition hole was drilled in the highly stressed floor and then pressurized by use of a water-filled bladder. A second full-scale hole was drilled at 1.0 m distance from the first one. This formed a slender pillar between the holes. Four vertical rod-shaped heaters were installed close to the side of the pillar. The tangential stress in the pillar could be increased by increase of the heat load and by reduction of the support pressure in the bladder. In the second hole, spalling occurred as response to excavation. Each of the measures taken to increase the tangential stress, i.e. heating and bladder pressure reduction, extended the breakout zone further down the hole. To reduce heat loss, the tunnel floor above the experiment volume was covered by insulation.

Figure 1-1 shows the experiment geometry in a schematic way. Temperatures were recorded at 18 positions on the walls of the two deposition holes, and in 10 positions in the rock.

The heat output required to generate the target thermal stresses was determined using results from preliminary thermo-mechanical calculations /Wanne and Johansson, 2003; Fredriksson *et al*., 2003; Andersson, 2004; Fredriksson *et al.*, 2004; Rinne *et al.* 2004; Wanne *et al*., 2004/. During the course of the experiment, the measured temperatures were found to be much lower than the predicted ones. In addition, the right-hand side temperatures turned out to be lower than the left-hand side temperatures. Therefore the power of the heaters was changed at a number of times during the course of the experiment. The bladder had a constant pressure of 0.7 MPa until it was depressurized at a certain time close to the end of the experiment.

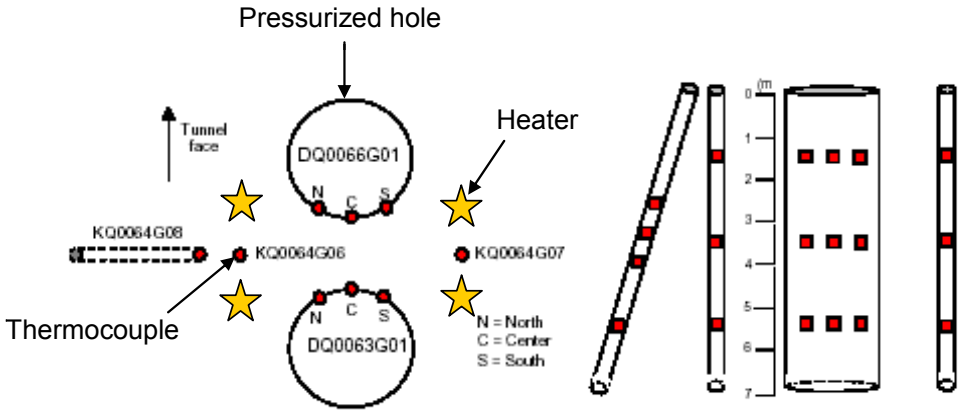

Figure 1-1. *Schematic view of the experiment. The left picture shows the location of the heaters and thermocouples in a horizontal plane. To the right is a vertical cut showing the locations of the thermocouples. KQ0064G08 is the inclined hole.*

2 Objectives and concerns

There were two main objectives of this work. The first was to back-calculate the temperature field in the pillar, using the temperature records as input. The second was to use that temperature field to find (or estimate) the thermal stresses in the pillar, i.e. without consideration of the in-situ stresses or the excavation-induced stress redistribution. The rock was assumed to be linearly elastic.

The results of the study may contribute to the work now going on to estimate the spalling strength of the APSE rock and to improve the general understanding of the spalling phenomenon. However, the final evaluation of APSE is a complex issue that will have to take in-situ stresses, excavation-induced stresses and the disturbance caused by spalling (and possibly other inelastic deformations) during the excavation phase into account.

In APSE the spalling process involved only small volumes of rock close to the periphery of openings. Therefore the numerical model needs to have a particularly fine mesh in the deposition hole wall regions. The problem is three-dimensional in nature. In addition, the geometry of the experiment is non-symmetric. Thus, there are no symmetry planes which can be used to reduce the model dimensions. This required a fully three dimensional model with a large number of elements.

3 Modeling approach

The modeling approach was to reproduce the temperature field in the experiment region using

- the temperature records obtained from the walls of the two deposition holes (DQ0063G0, DQ0066G01) as time-dependent boundary conditions
- the temperature records from the rock (KQ0064G06, KQ0064G07) together with approximate values of the temperature found between the tunnel floor and the floor thermal insulation to calibrate rock thermal properties (i.e. the rock thermal conductivity) and boundary conditions (heat transfer to the tunnel air).

In reality, heat transport in fractured rock close to drained excavations at great depth is not a simple question of linear heat conduction. This is the reason why the input effective heat conductivity must be calibrated rather than just set to the nominal value. No attempts are made here to account for any spatial variation of the effective heat conductivity.

During the experiment, extensive water movements were observed in the right part of the experiment. At times, there were also observations of steam. In the modeling work described here, no efforts were made to capture any of this explicitly. Instead the heat loss was accounted for by reducing the right side power below the given nominal values.

When a reasonable fit between measured and calculated temperatures was obtained, the thermally induced stress state in the pillar was calculated.

The 0.7 MPa pressure in the hole closest to the tunnel face was not included in the analysis since it does not contribute by more than about 1 % to the pillar stress field.

Below follows a discussion of how the parameter values used in the model were obtained, and how some observed processes were modeled.

3.1 Thermal conductivity

Eq. 3-1 below gives the temperature $T_{rock}(r,z,t)$ at different points around a line heat source in a homogeneous isotropic medium:

$$T_{rock}(r,z,t) = \frac{Q}{4\pi\lambda_r} \cdot \int_{-H_c}^{H_c} \left\{ \frac{1}{\sqrt{r^2+(z'-z)^2}} \cdot erfc\left[\frac{\sqrt{r^2+(z'-z)^2}}{\sqrt{4at}} \right] \right\} dz' \qquad (3\text{-}1)$$

This equation is readily obtained by integration of corresponding textbook point source solutions along the length of the line source, see for instance Claesson, 1996. Here Q is the power per unit length, λ_r the thermal conductivity, a the thermal diffusivity, and t the time after the heating started. H_c is the source half-length and r and z are the point coordinates (see Figure 3-1, right). The heat transport must be assumed to be linear heat conduction. Simultaneous contributions from many line sources can be considered using the principle of superposition, /Hökmark and Fälth, 2003/.

The analytical solution was used to examine the temperature field close to the two line sources on the left side of the experiment over the first days. The results were used to calibrate a relevant value of thermal conductivity, λ, for use in the numerical model. Figure 3-1 (left) shows the analytically obtained results along with the experimental data at the measuring point (KQ0064G06) between the left pair of heaters at 1.5 m depth.

As Figure 3-1 shows, the nominal value of λ =2.6 W/(mK), obtained from Staub *et al*. 2004, was found to overestimate the temperature. For λ =3.2 W/(mK) the analytical model was in better agreement with the measured temperature.

The estimate of the thermal conductivity, obtained by the analytical study, was found to be appropriate also in numerical finite element analyses. Both 2D and 3D finite element models showed good agreement with experimental data when using the analytical estimate.

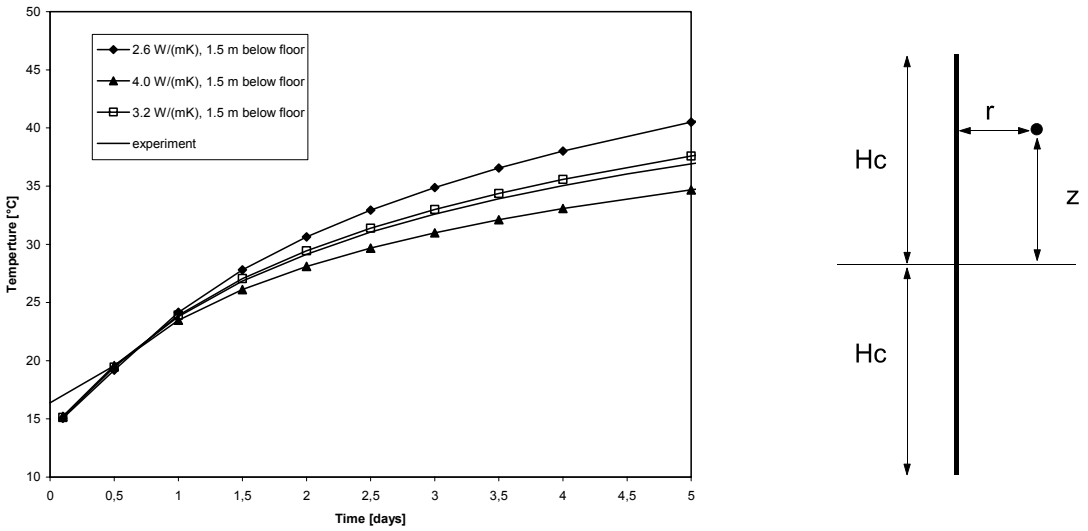

Figure 3-1. *Left: Temperatures between the two left heaters as function of time. Right: geometry of line source.*

3.2 Tunnel insulation

To investigate what convection heat transfer coefficient, γ, to use in the model at the isolated part of the tunnel floor, the model was calibrated against the measured mean temperature 36.5 °C, which was found under the insulation at the tunnel floor between the left pair of heaters between day 40 and day 53. The model corresponds well with the experiment for γ=0.5 W/(m^{2}K) at the isolated part of the tunnel, which can be seen in Figure 3-2, where the temperature is shown for points between the left pair of heaters. The rest of the tunnel was given the value γ=10 W/(m^{2}K).

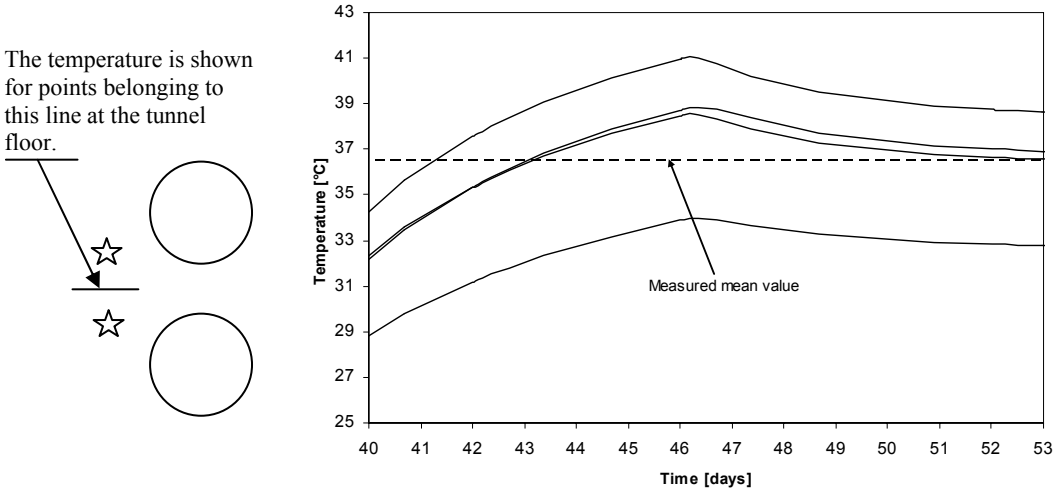

Figure 3-2. *Simulated temperature at the tunnel floor between the left pair of heaters.*

3.3 Water-bearing fracture on the right side

Water-bearing fractures were observed at the right side of the pillar. This resulted in cooling of this side which is clearly seen in the experimental measurements when comparing the left and right side data, see Figure 3-3. To compensate for this in the simulation, the heater power on the right side heaters was overall decreased by 20 W/m. With this heater power reduction, the simulated temperature agreed well with experimental measurements between the right heater pair until day 42 in the experiment.

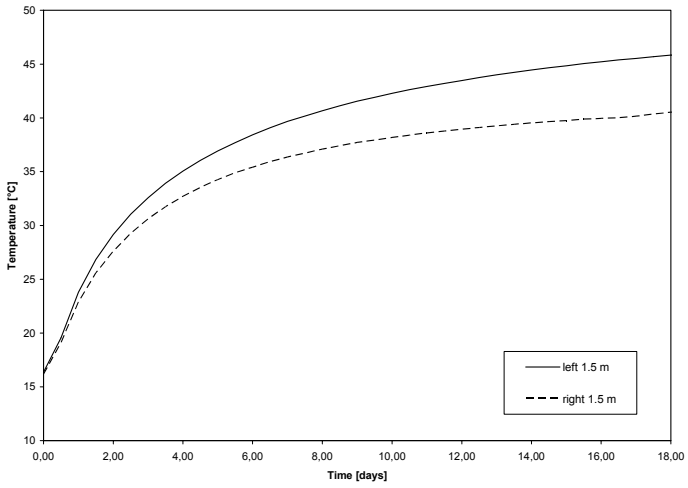

Figure 3-3. *Measured temperatures in KQ0064G06 (left) and in KQ0064G07 (right) at 1.5 m depth.*

3.4 Boiling on the right side

At day 42 in the experiment, steam was observed coming up from the right-hand side heaters. In the experimental right-hand side measurements, a reduction in temperature can be seen at this instant, see Figure 3-4. To compensate for the extra power loss, the heater power was reduced by 80 W/m, in addition to the over all reduction of 20 W/m made to compensate for water movements on this side.

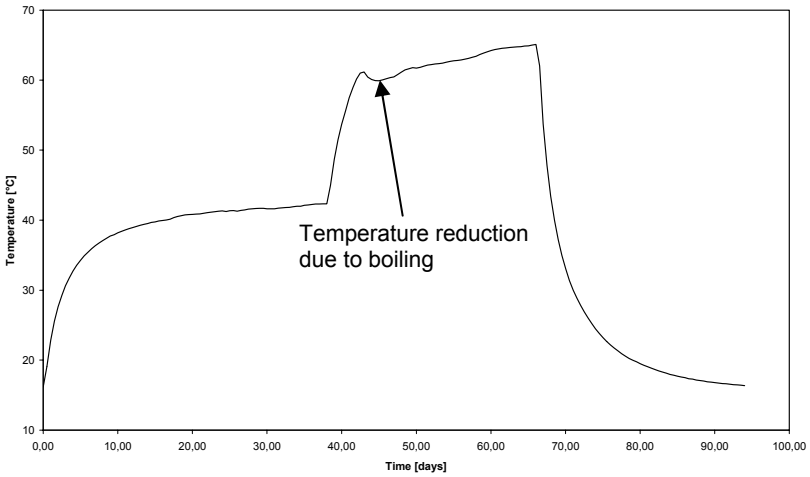

Figure 3-4. *Measured temperature between right heater pair (KQ0064G07) at 1.5 m.*

4 Model description

4.1 General

Code_Bright, a finite element code developed at the University of Barcelona /CIMNE, 2000/, was used to model the problem. In order to obtain a geometrical model of the experimental setup, the problem was formulated in three dimensions.

4.2 Geometry

A three-dimensional geometry of the experiment was developed which accounted for individual positions and dimensions of holes, heaters and thermocouples,. The model of the experiment geometry was surrounded by a large volume of material, the embedment (see Figure 4-1), in order to avoid influence from the thermal and mechanical constraints at the boundary of the embedment.

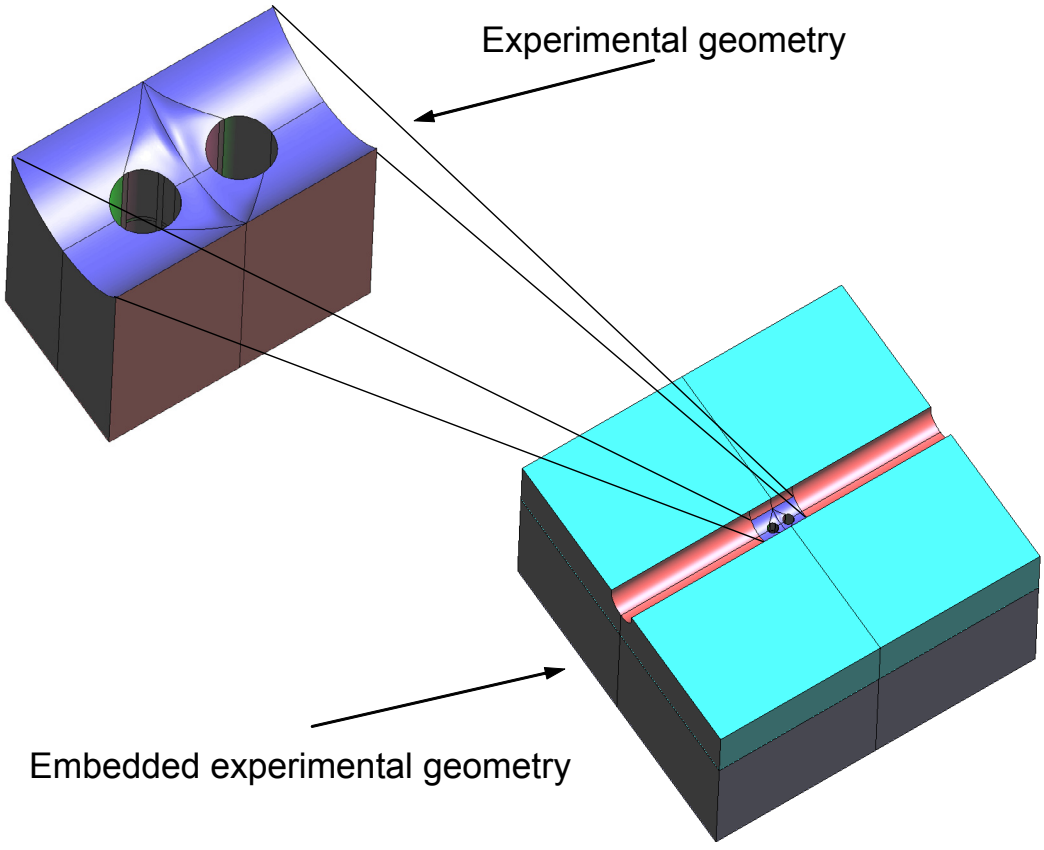

Figure 4-1. *The experiment geometry, free and embedded.*

The mesh, shown in Figure 4-2, consisted of 99517 tetrahedral elements, and 19233 nodes. The mesh was most dense at the pillar center and at the heater positions and gradually becomes coarser with increasing distance from the center of the geometry. The element size was set to 0.06m at the pillar center.

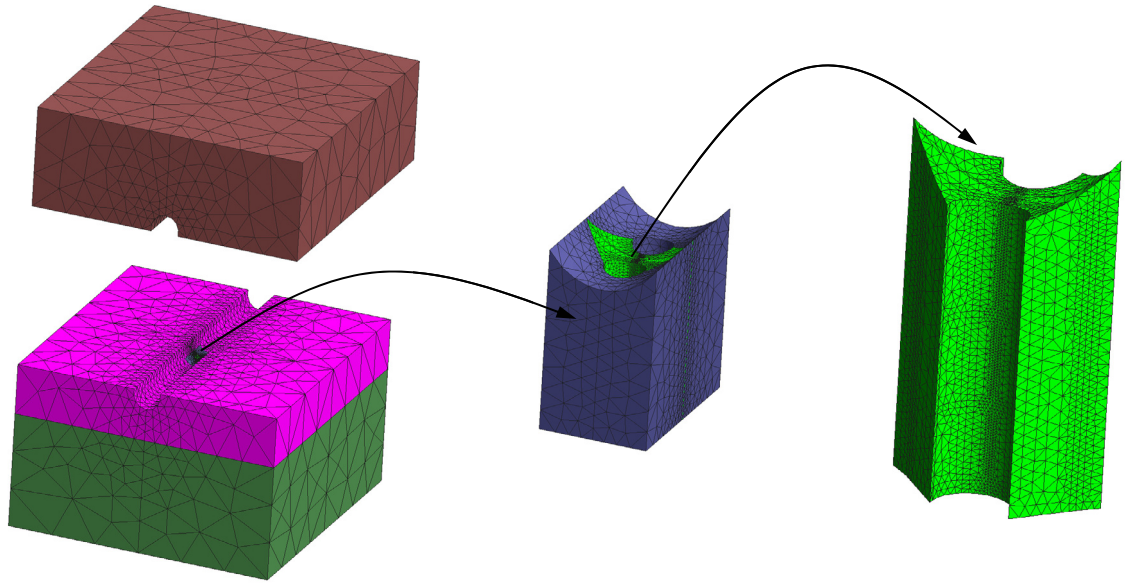

Figure 4-2. *The model mesh.*

4.3 Material

A linear elastic mechanical material model with linear thermal expansion was adopted for the rock material. Linear heat conduction was used. With exception of the thermal conductivity value, the parameter values were obtained from /Staub *et al*., 2004/. The thermal conductivity value was obtained from a calibration against temperature measurements, c.f. section 3.1. The parameters in the model are given in Table 4-1.

Table 4-1. Material parameters used in the model.

E [GPa]	v	α [1/K]	ρ [kg/m^3]	λ [W/(mK)]	C [J/(kgK)]
76	0.25	7 10^{-6}	2277	3.2	770

4.4 Thermal load

The thermal load was adjusted in accordance with the description given in section 3. An overall reduction of the right-hand pair heater power of 20 W/m and an additional reduction of 80 W/m beginning at day 42 were found to reproduce the recorded temperatures well. In Table 4-2, the heater powers used in the left- and right-hand heater pairs are presented along with the corresponding powers used in the experiment.

Table 4-2. Heater powers used in the experiment and in the model. Note the power reductions made in the right-hand side heaters.

Days from heater startup	Left [W/m]		Right [W/m]	
	Experiment	Model	Experiment	Model
0	200	200	200	180
18	170	170	200	180
38	354	354	400	380
42	354	354	400	300
46	263	263	400	300
66	0	0	0	0

The asymmetric heater configuration has been considered in the model as can be seen in Figure 4-3. Both left-hand heaters and the "lower" right-hand heater have similar heated length, 6.50 m, and the same vertical position, with 6.35 m as maximum depth. The "upper" right-hand heater, which starts at the tunnel floor, has an effective heated length of 5.61 m, with its deepest point at 4.80 m.

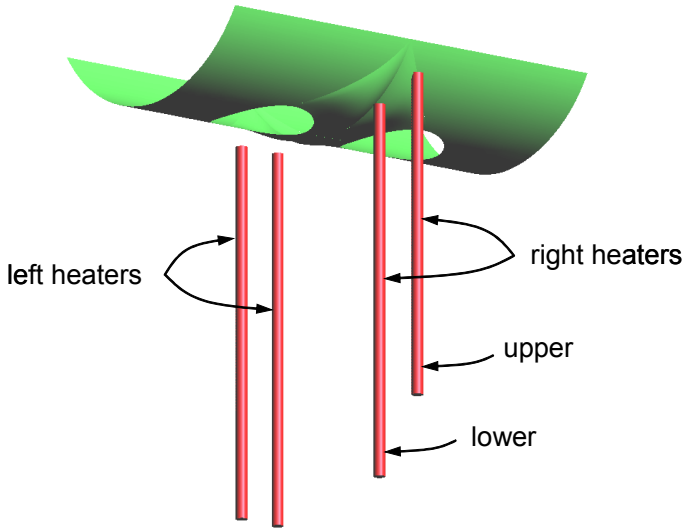

Figure 4-3. *Model geometry of the heaters.*

4.5 Boundary conditions

4.5.1 Mechanical boundary conditions

The mechanical boundary conditions used at the boundary of the embedment are indicated in Figure 4-4. The top boundary and opening walls were free, i.e. the traction vector was prescribed to zero. The other embedment boundaries are not allowed to move in the normal direction to the surface but may move freely in the other directions.

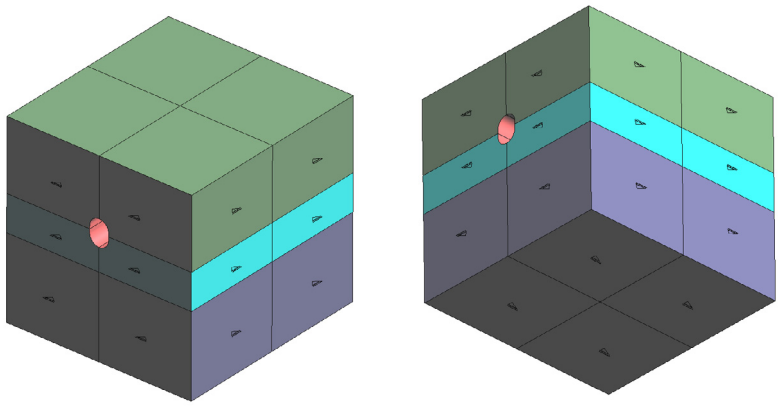

Figure 4-4. *Mechanical boundary conditions at the embedment boundaries.*

4.5.2 Thermal boundary conditions

At the embedment boundary, the thermal boundary conditions were prescribed as adiabatic.

The tunnel has two areas with different convection boundary conditions, which are indicated in Figure 4-5. At the top of the experimental volume, where the tunnel floor was insulated during the experiment, the convection heat transfer coefficient was prescribed to 0.5 W/(m^2K). Everywhere else in the tunnel the convection heat transfer coefficient was prescribed to 10 W/ (m^2K).

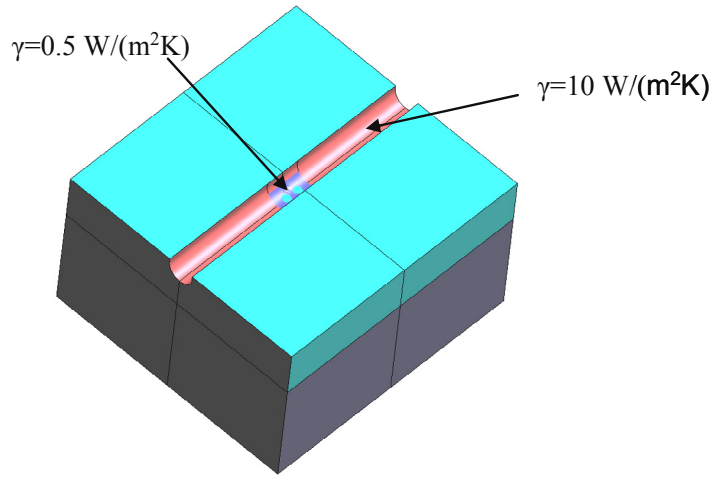

Figure 4-5. *The tunnel where the areas with different convection boundaries are indicated.*

According to Figure 1-1, the temperature was measured in nine points at the wall of each deposition hole (north, center and south and at 1.5 m, 3.5 and 5.5 m depth). The temperature difference between the north-, center- and south locations was judged to be small. Thus, only the "center" measurements were used as boundary conditions in the model. The "face" hole wall area in each deposition hole was divided into three sections corresponding to 1.5 m, 3.5 m and 5.5 m depth, respectively (Figure 4-6). At each section, the "center" temperature history at that depth was applied as a time dependent boundary condition. The "back" of the hole wall area has the corresponding center temperature at 3.5 m depth prescribed as boundary condition. The bottoms of the holes had adiabatic boundary conditions.

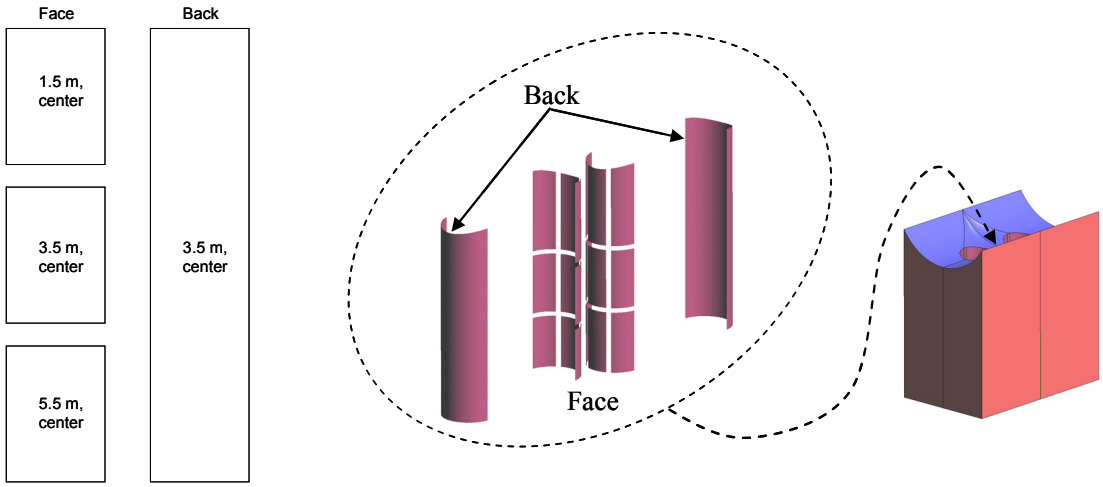

Figure 4-6. *Areas with temperature boundary conditions in the holes.*

5 Results

Results are shown for the model described in the previous section. First the reproduced temperature field is shown at day 38 and day 52 in a left side view and in a horizontal plane at 1.5 m depth, Figure 5-1 - Figure 5-5. Calculated temperatures are also shown together with the corresponding measurements in Figure 5-6 - Figure 5-8. Then follows representations of the stress normal to the tunnel direction at day 38 and 52 in Figure 5-9 - Figure 5-17, and the stress history at points in the pillar, Figure 5-18 - Figure 5-20. The displacement vector field projected on a horizontal plane at 1.5 m depth at day 38 and day 52 is shown in Figure 5-21 and Figure 5-22, respectively, and the displacement history is shown at points at the hole walls in Figure 5-23 and Figure 5-24.

In the figures where the left side view or horizontal plane are shown, the tunnel face is to the right.

5.1 Temperature response

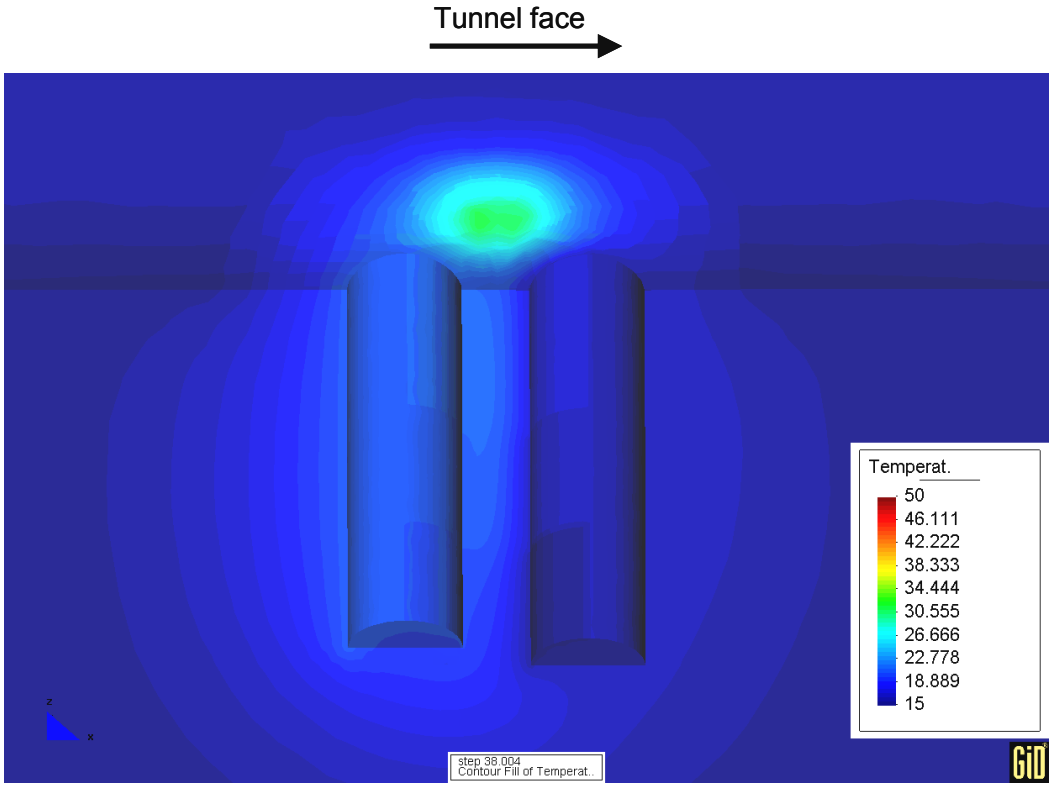

Figure 5-1. *Temperature map of the left side of the model at day 38.*

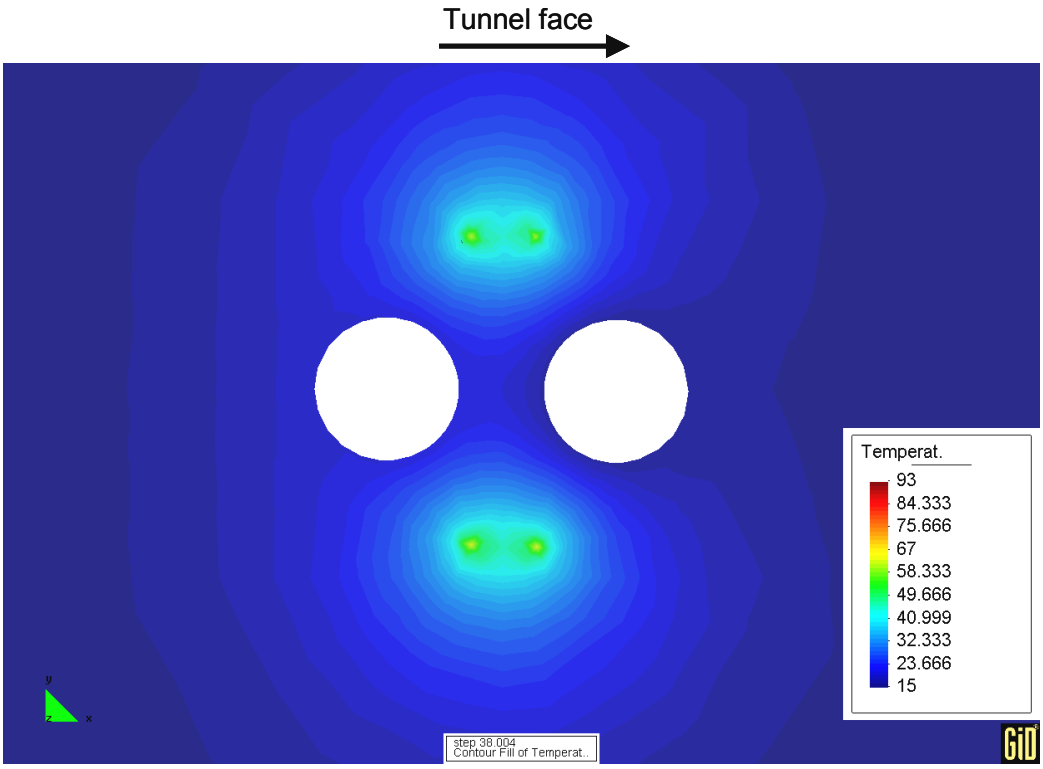

Figure 5-2. *Temperature at 1.5 m depth, day 38.*

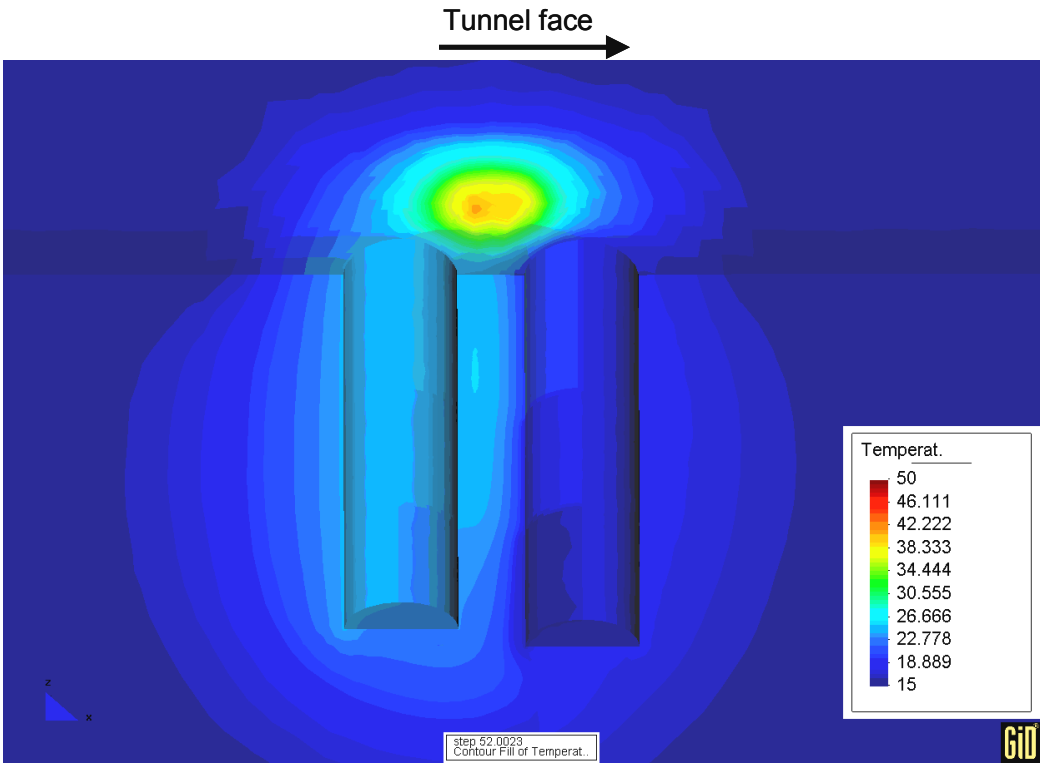

Figure 5-3. *Temperature map of the left side of the model at day 52.*

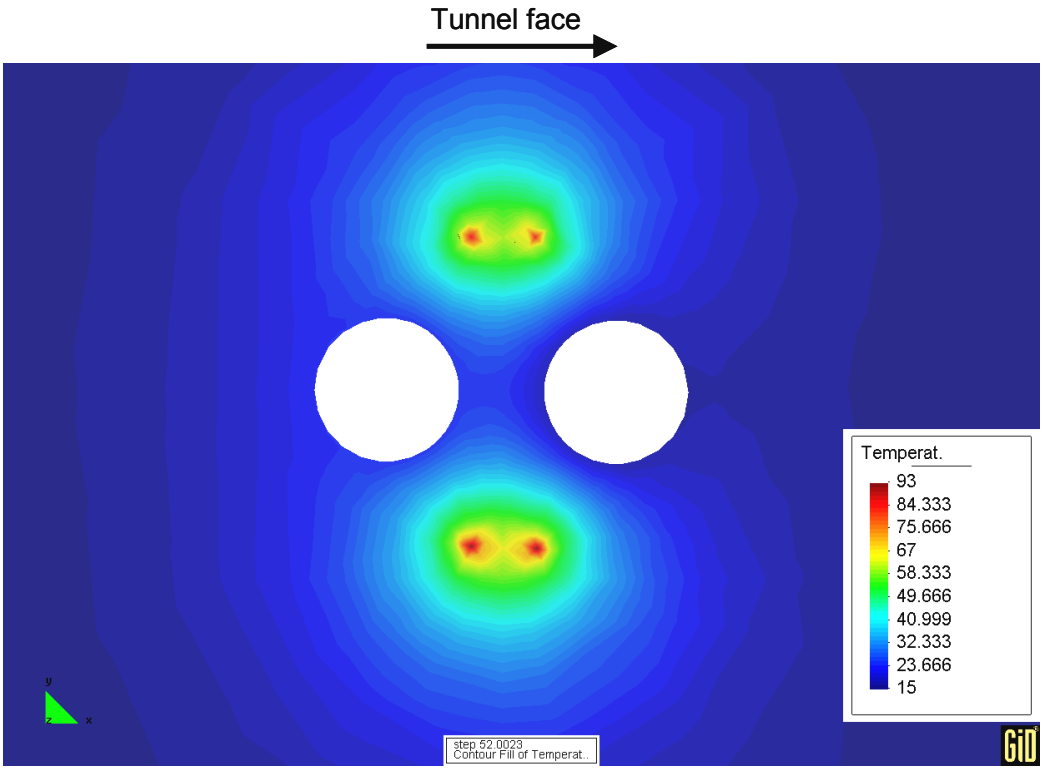

Figure 5-4. *Temperature at 1.5 m depth, day 52.*

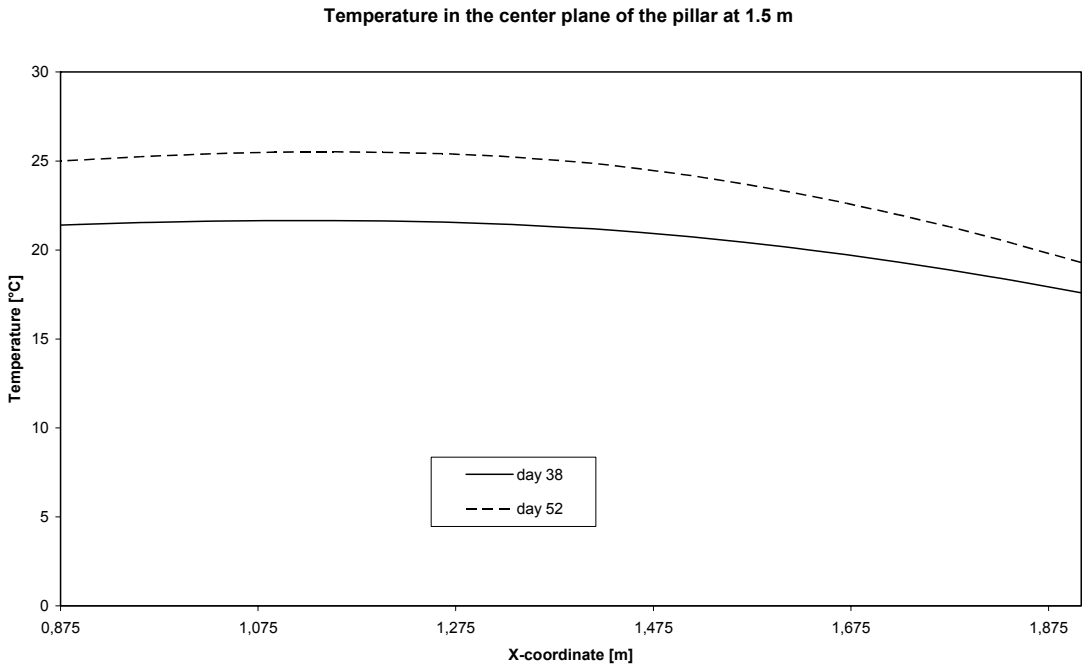

Figure 5-5. *Temperature in the center plane of the pillar at 1.5 m depth.*

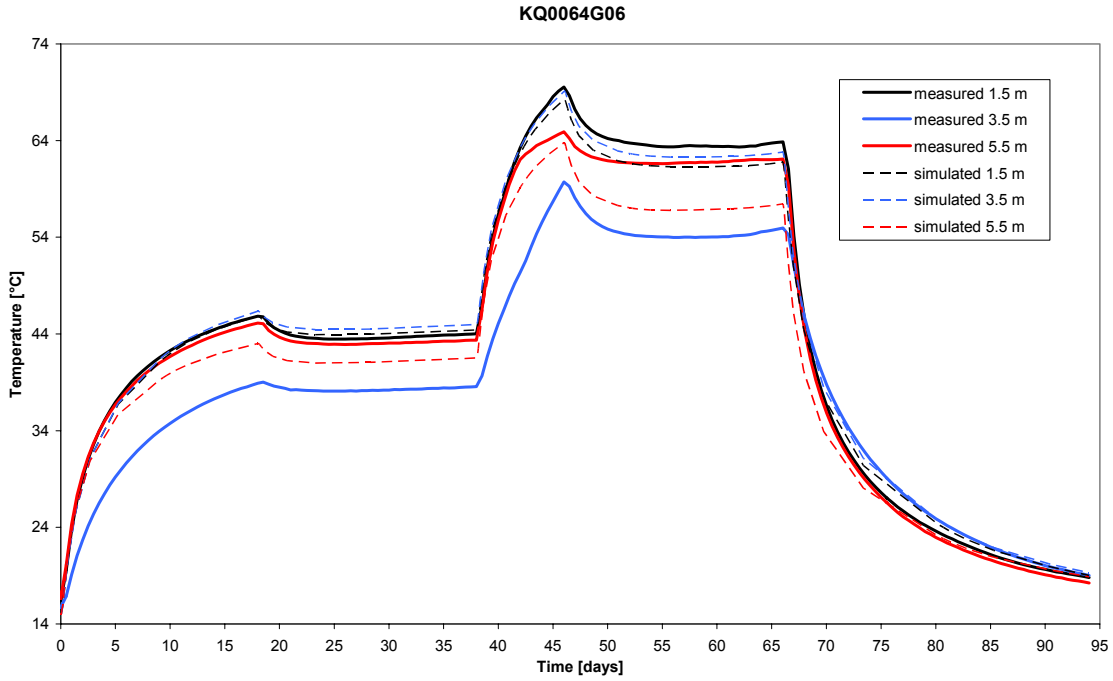

Figure 5-6. *Measured and simulated temperature histories between the left heaters.*

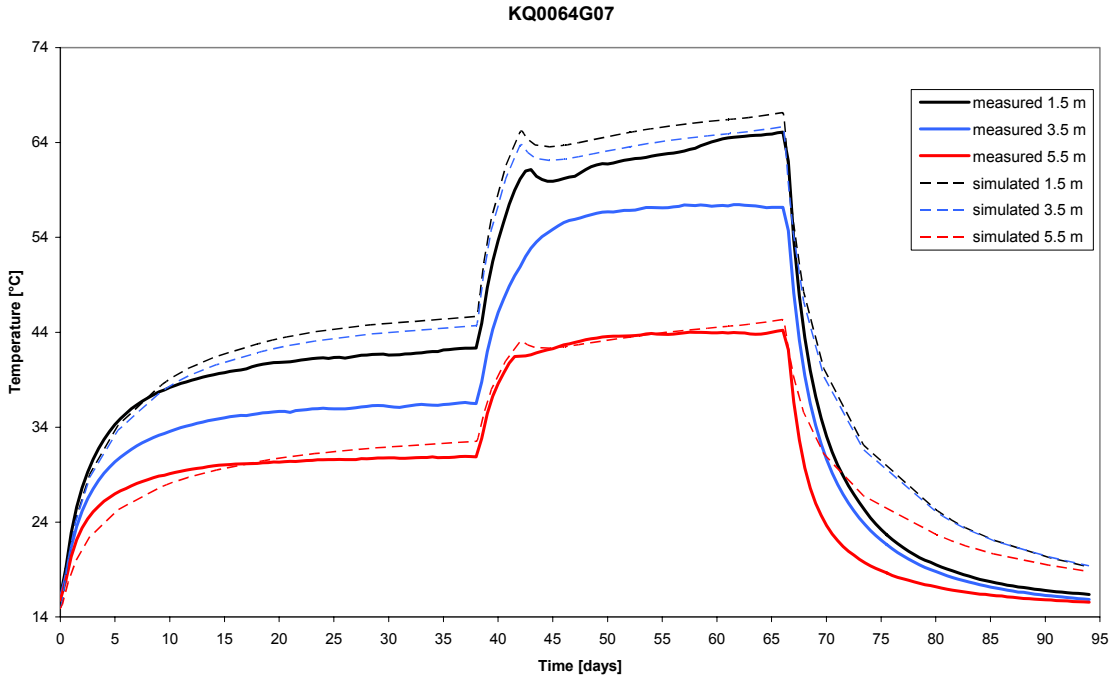

Figure 5-7. *Measured and simulated temperature histories between the right heaters.*

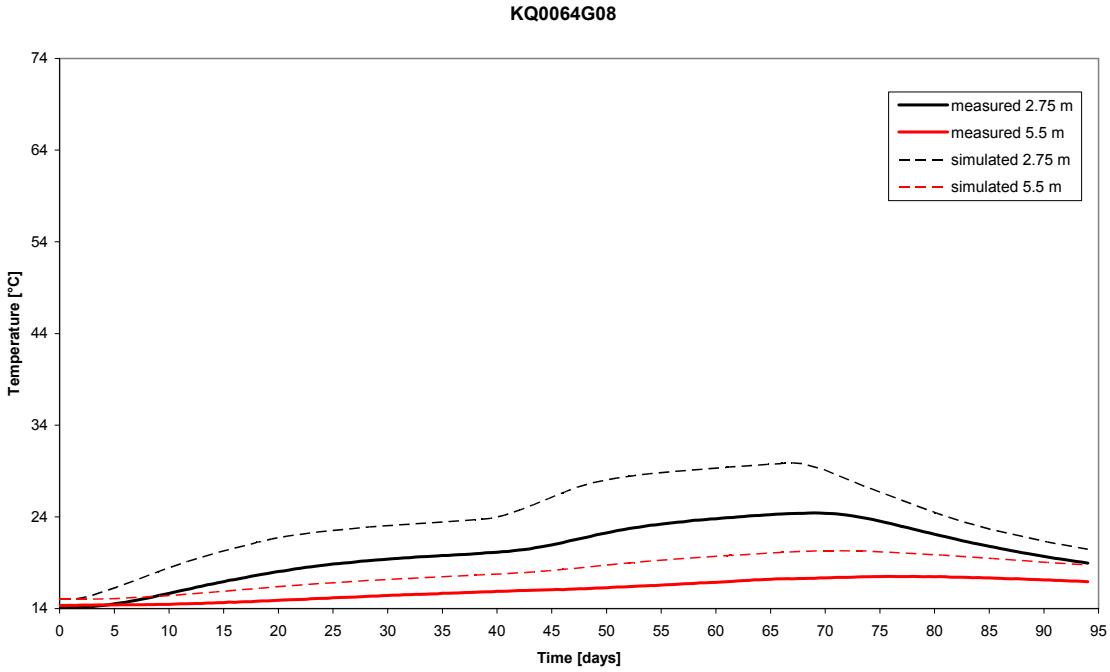

Figure 5-8. *Inclined bore hole at the left side. Measured and simulated temperature histories.*

5.2 Stress response

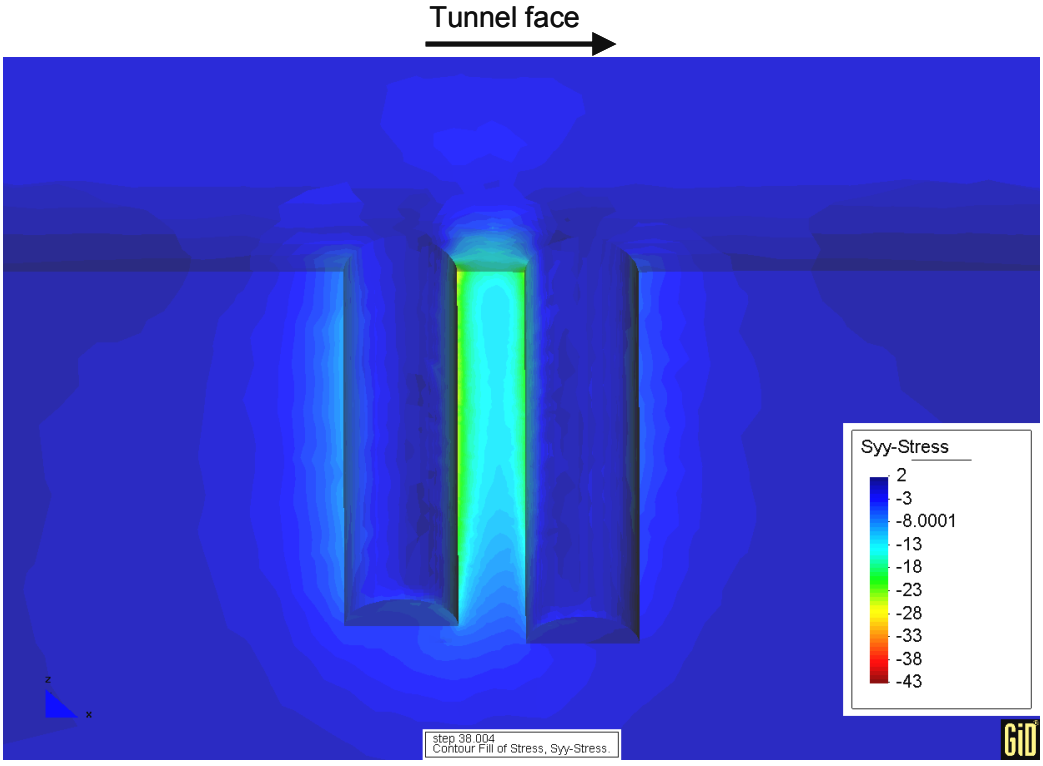

Figure 5-9. *Map of the stress component normal to the tunnel direction at day 38.*

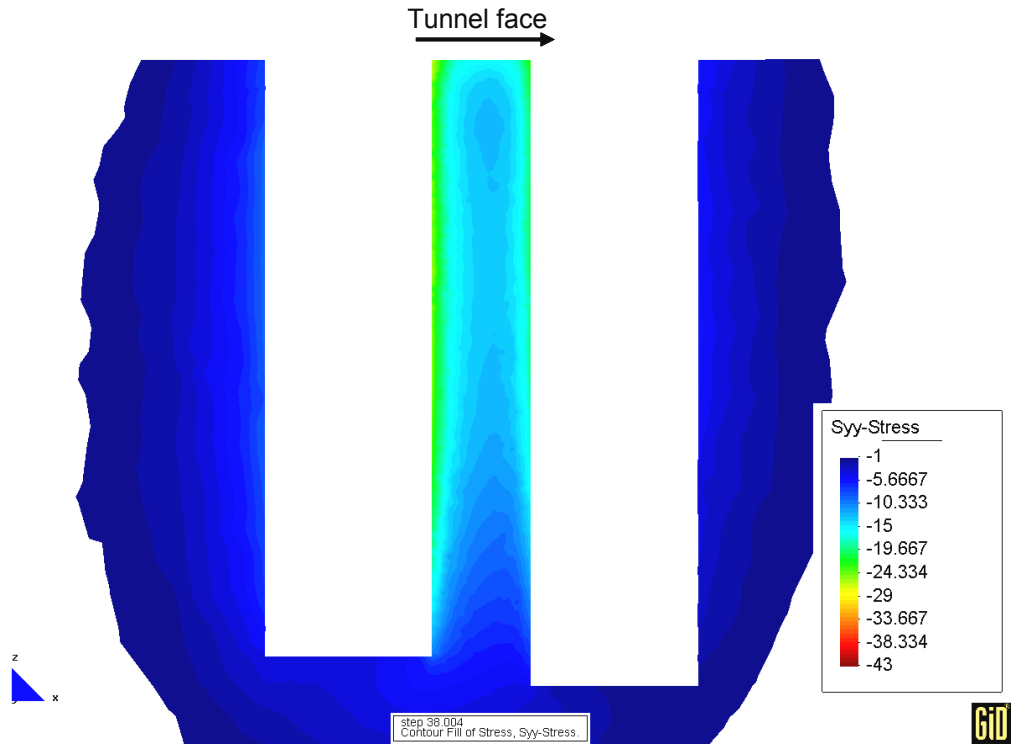

Figure 5-10. *Map of the stress component normal to the tunnel direction at day 38, a close-up of the pillar.*

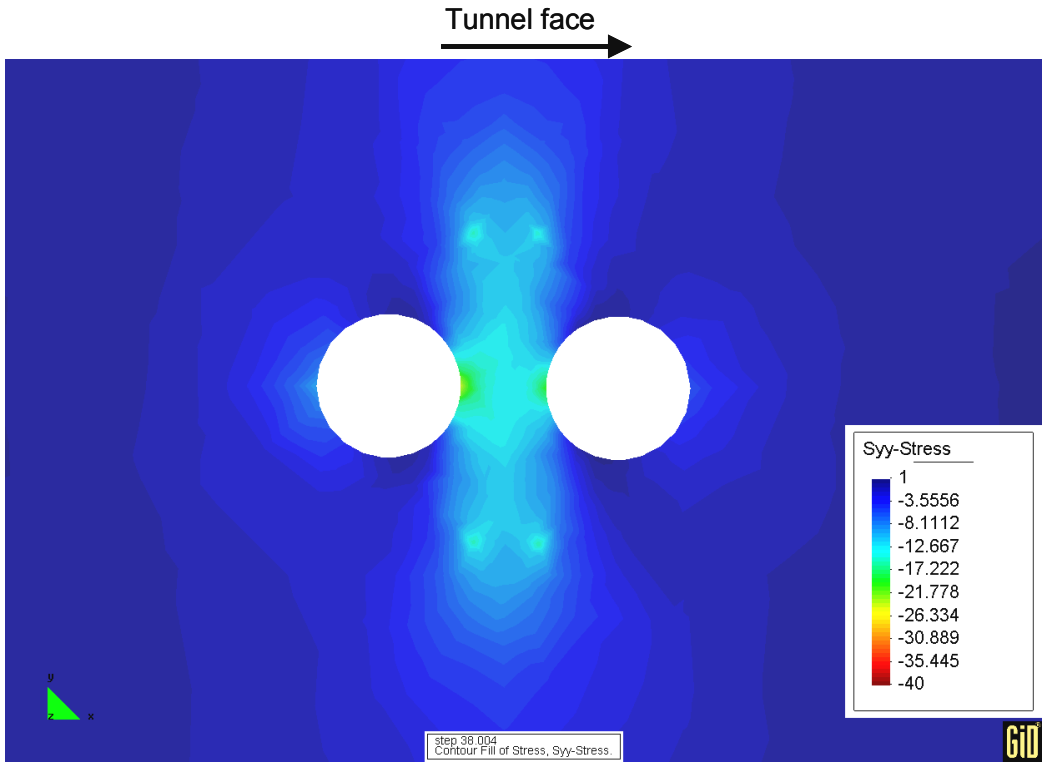

Figure 5-11. *Stress component normal to the tunnel direction at 1.5 m depth, day 38.*

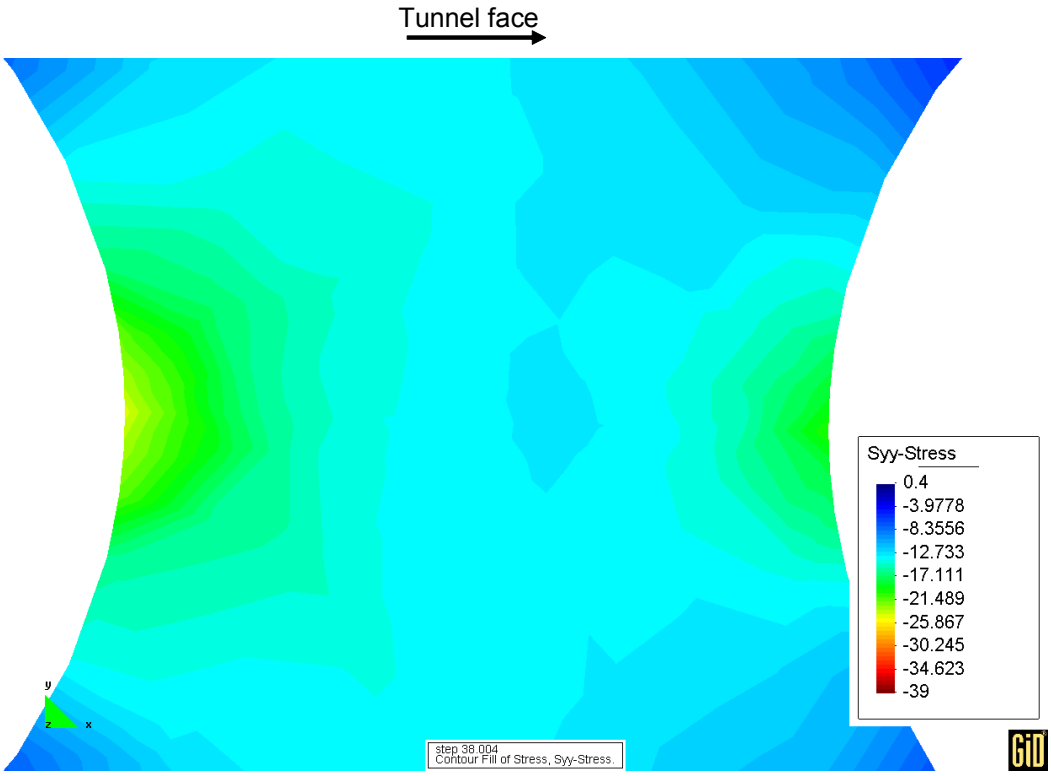

Figure 5-12. *Stress component normal to the tunnel direction at 1.5 m depth, day 38. Close-up of the pillar.*

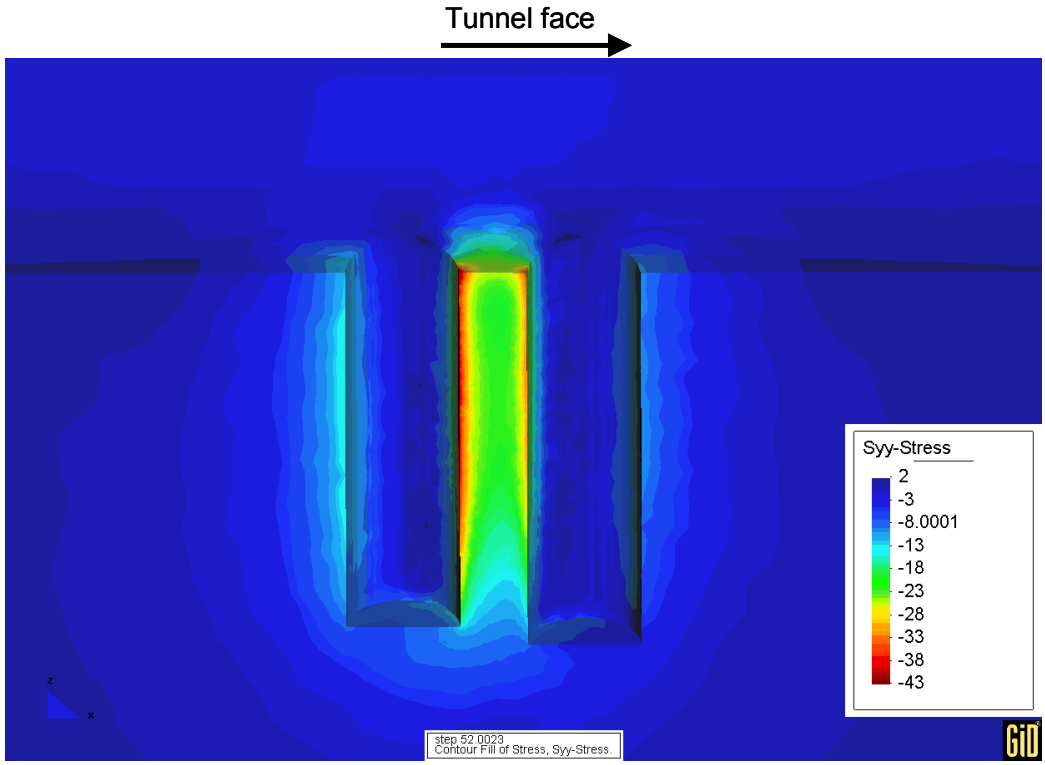

Figure 5-13. *Map of the stress component normal to the tunnel direction at day 52.*

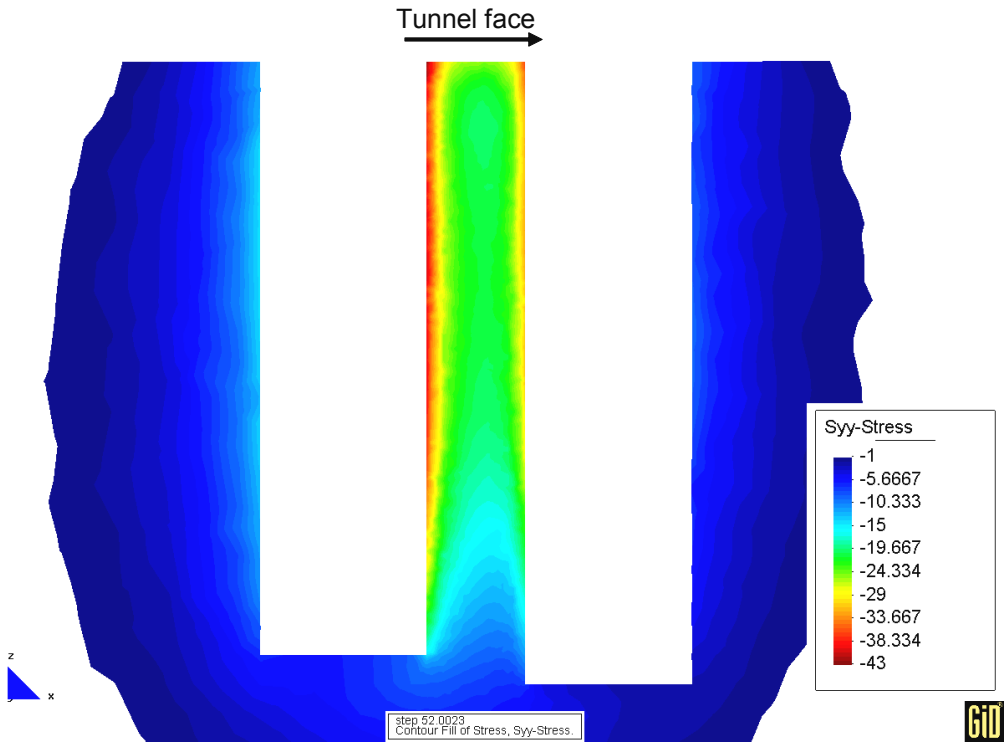

Figure 5-14. *Map of the stress component normal to the tunnel direction at day 52. Close-up of the pillar.*

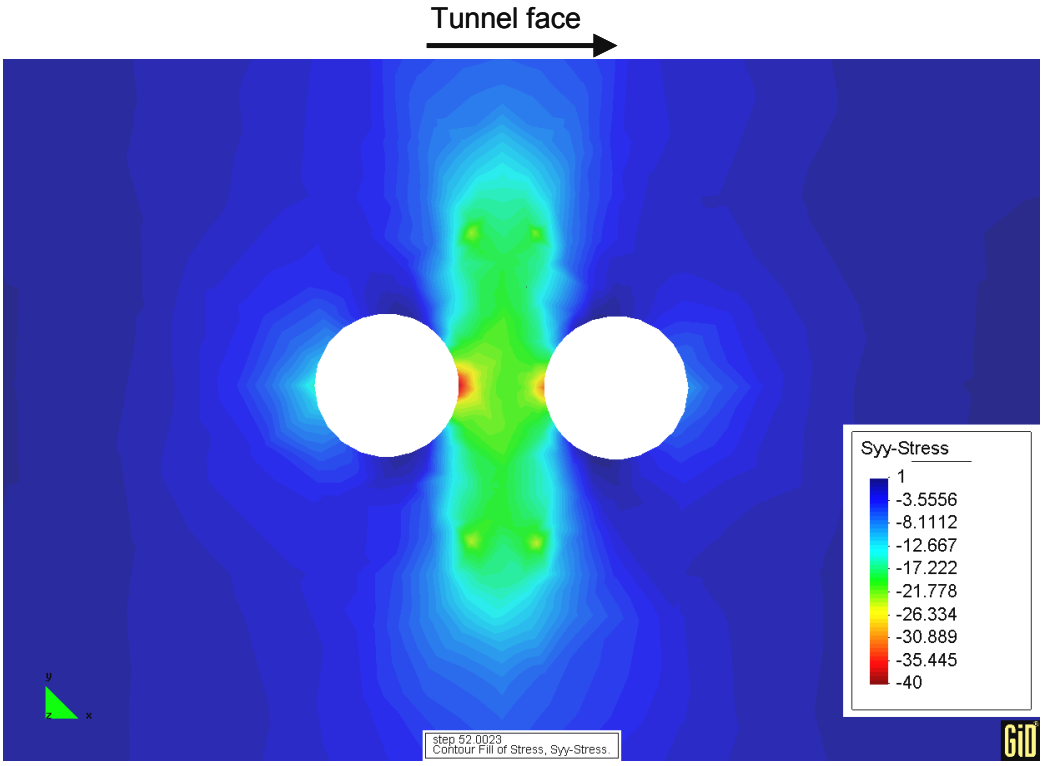

Figure 5-15. *Stress component normal to the tunnel direction at 1.5 m depth, day 52.*

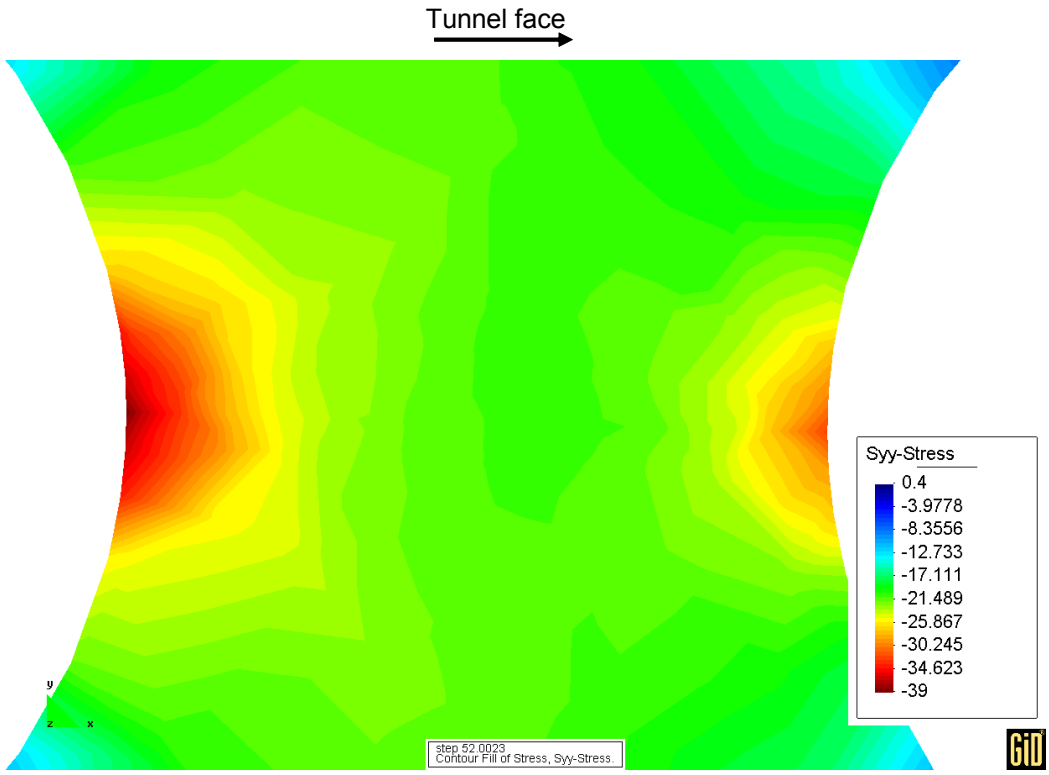

Figure 5-16. *Stress component normal to the tunnel direction at 1.5 m depth, day 52. Close-up of the pillar.*

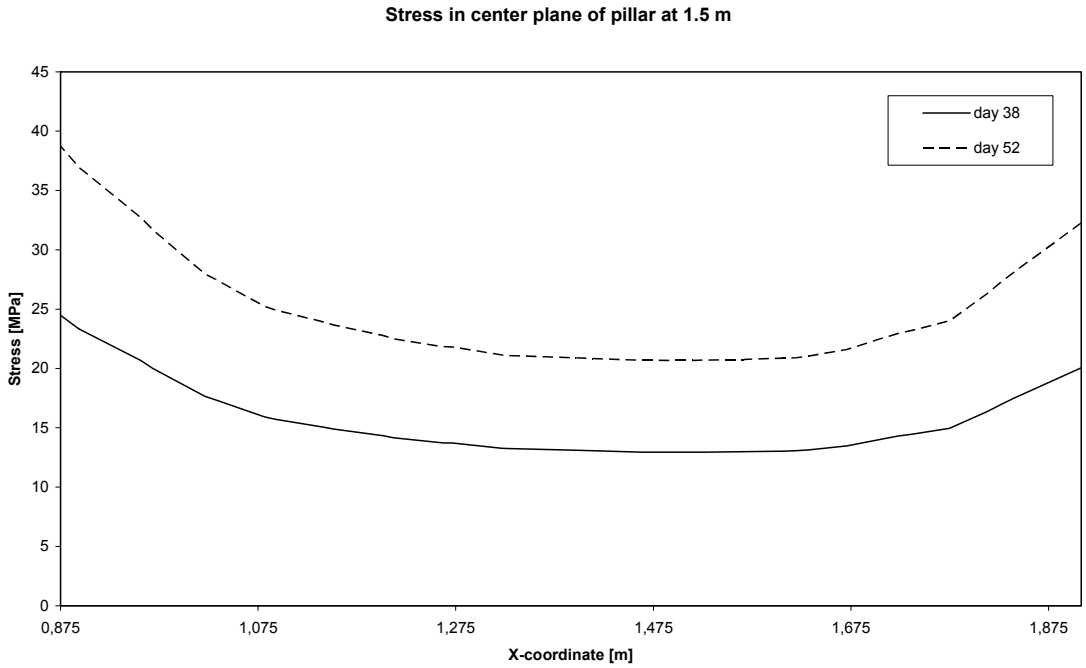

Figure 5-17. *Stress in the center plane of the pillar at 1.5 m depth.*

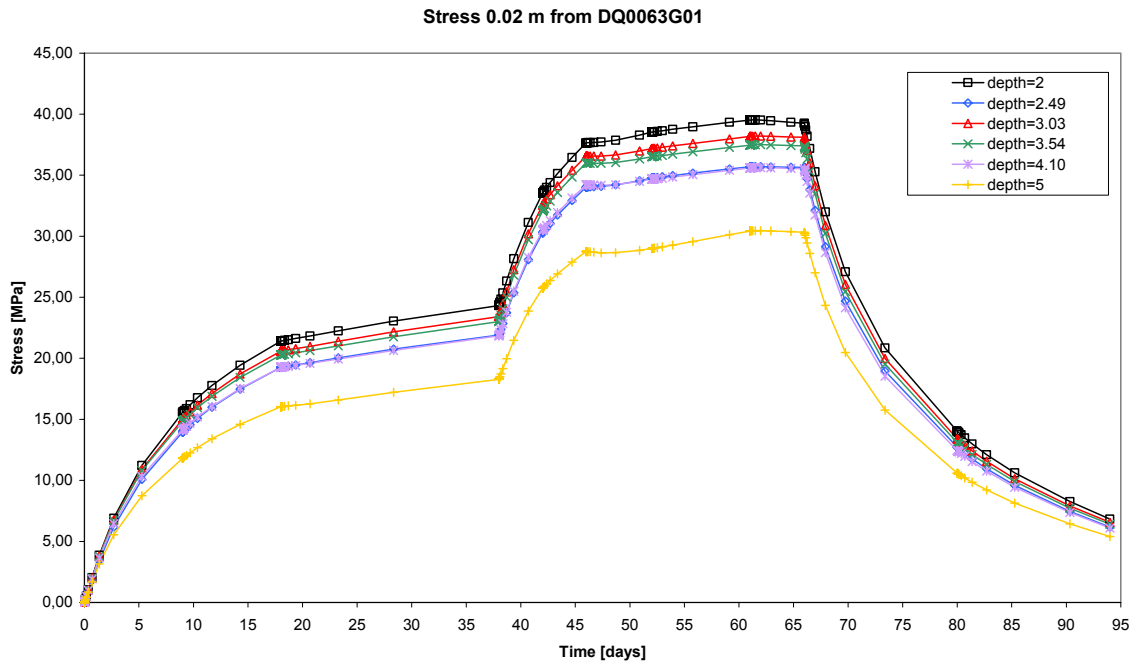

Figure 5-18. *Stress component normal to the tunnel direction at 0.02 m from DQ0063G01 in pillar.*

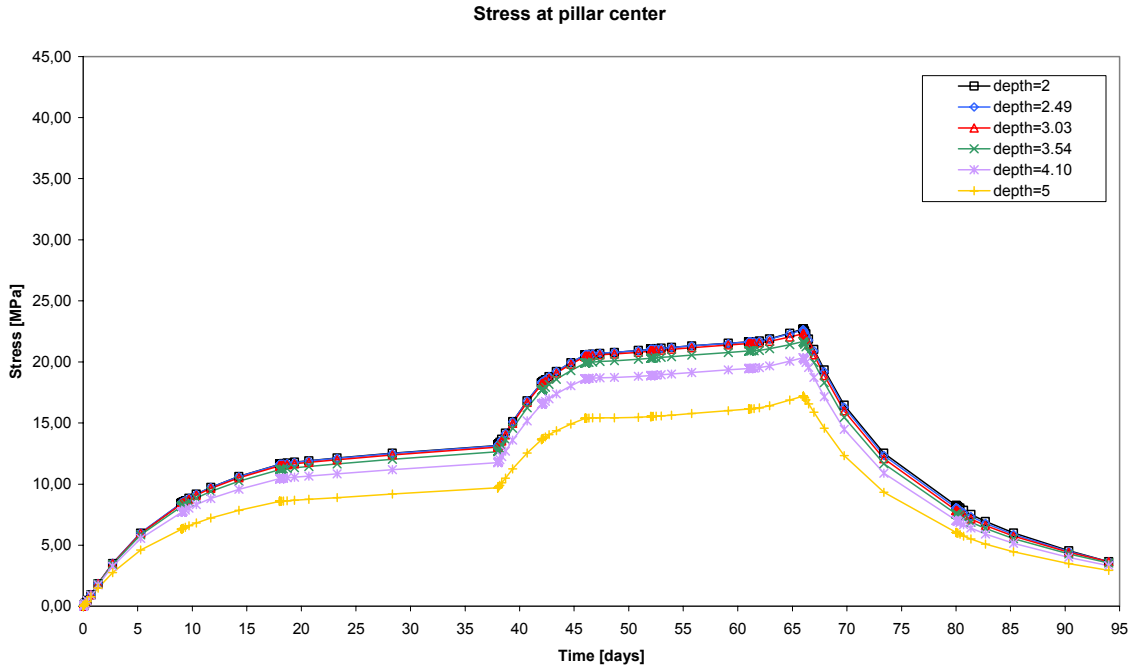

Figure 5-19. *Stress component normal to the tunnel direction at pillar center.*

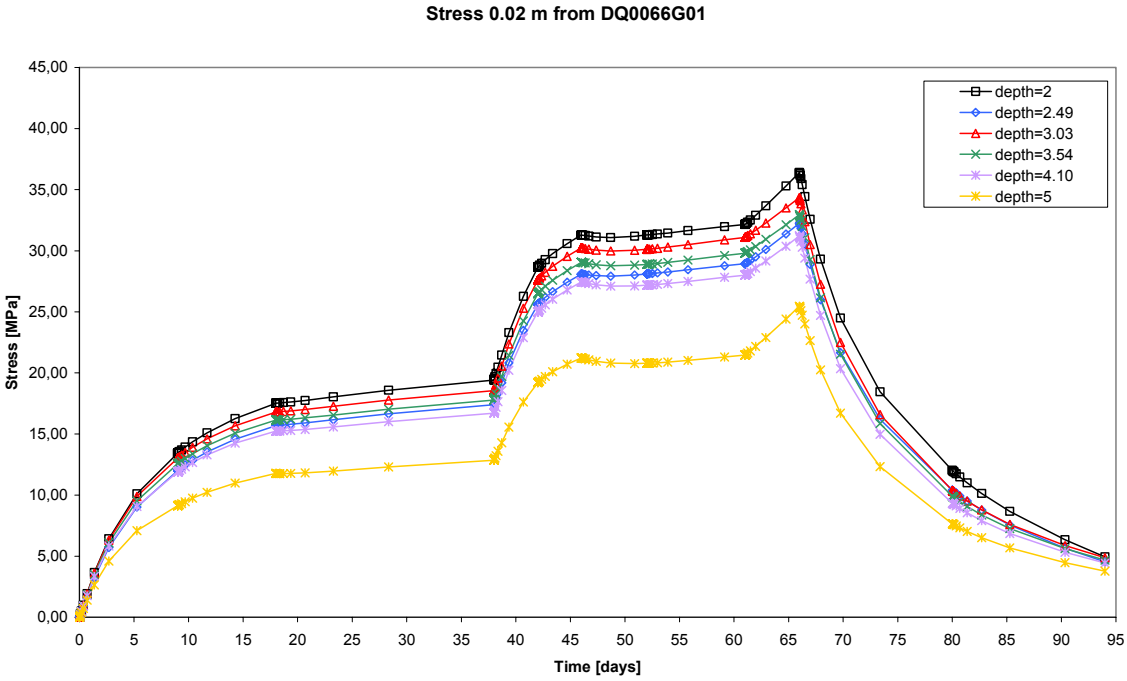

Figure 5-20. *Stress component normal to the tunnel direction at 0.02 m from DQ0066G01 in pillar.*

5.3 Displacements

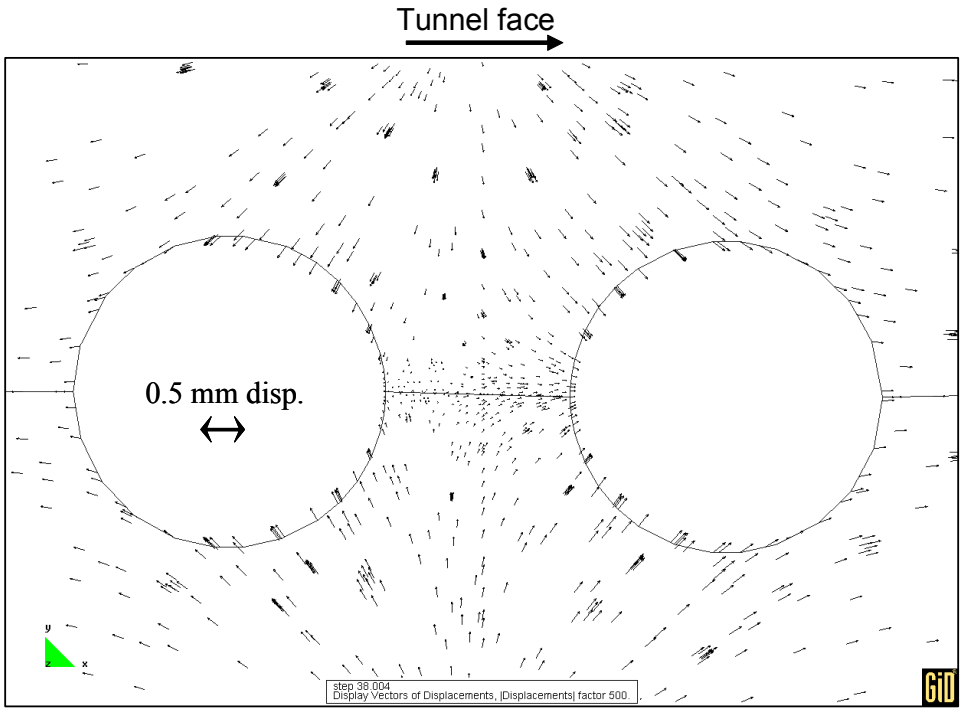

Figure 5-21. *Displacement vector field projected on a horizontal plane at 1.5 m depth, day 38.*

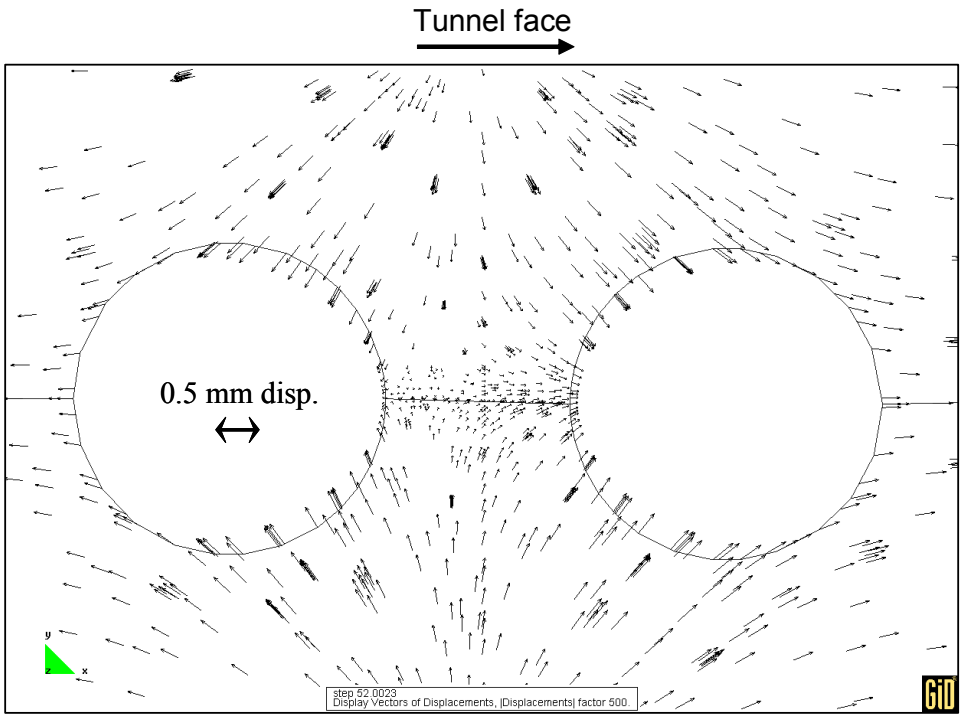

Figure 5-22. *Displacement vector field projected on a horizontal plane at 1.5 m depth, day 52.*

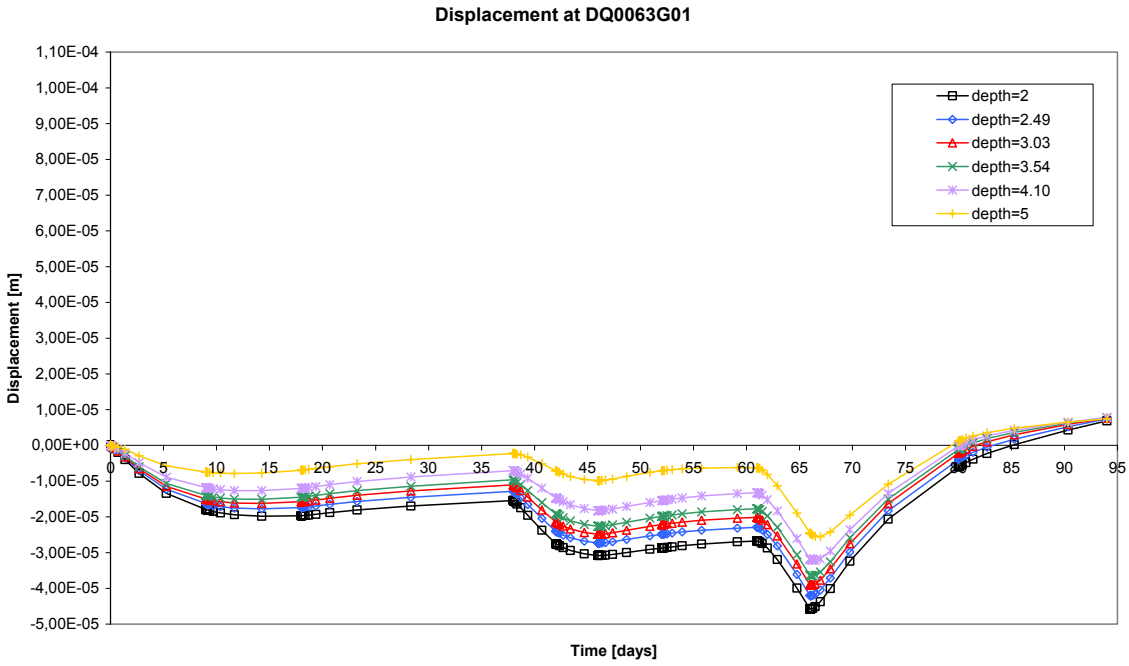

Figure 5-23. *Displacement histories at points on the hole wall of DQ0063G01.*

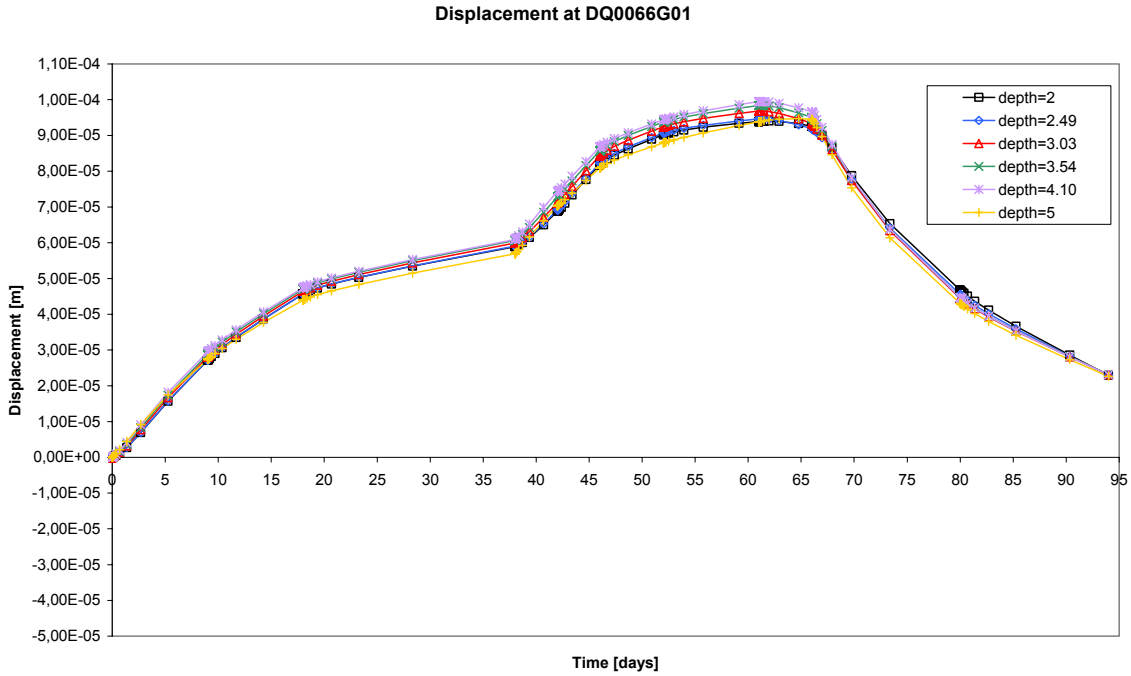

Figure 5-24. *Displacement histories at points on the hole wall of DQ0066G01.*

5.4 Sensitivity analysis

In addition to the base case analysis presented above, two other cases were also studied where the properties of the embedment were altered (see Figure 4-1).

- The influence of the over predicted temperature in the embedment, see Figure 5-8, on the pillar stress field was investigated.
- The influence from decreasing the Young's modulus in the embedment on the pillar stress field was studied.

5.4.1 Effects of overestimating temperatures outside the pillar region.

In the experimental geometry, which is the embedded geometry in Figure 4-1, the temperatures are rather well predicted; see Figure 5-6 and Figure 5-7. However, the simulated temperatures outside the experiment geometry showed too high values when compared with the experimental measurements (Figure 5-8). Figure 5-25 shows the position of the two measurement points used in Figure 5-8 in relation to the experiment volume. From studying Figure 5-8 the value 1.6 has been used as a measure of the relative temperature difference between simulated and measured temperatures. In order to compensate for the over estimated temperatures in the embedment the thermal expansion coefficient in the embedment was decreased to 1/1.6=0.625 of the nominal value.

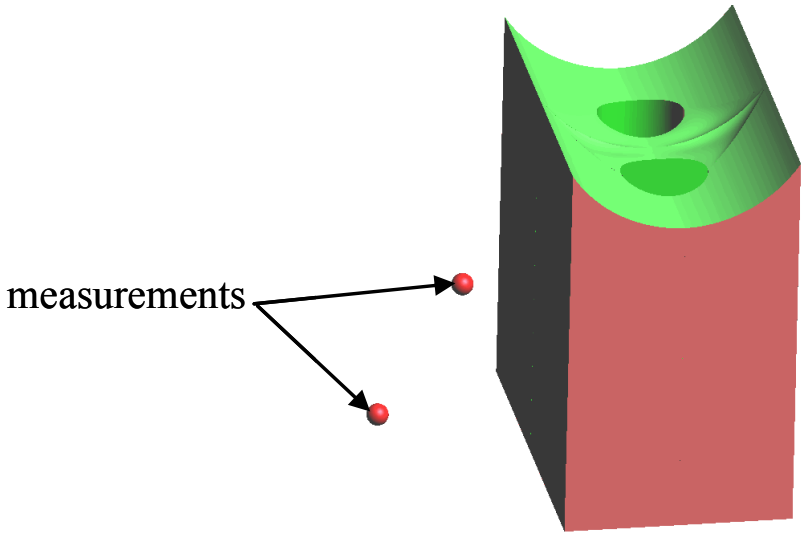

Figure 5-25. *Positions of the measurement points shown in Figure 5-8***.**

The analysis with the reduced thermal expansion coefficient showed that the maximal stress component normal to the tunnel direction decreased from 42.5 MPa to 37.7 MPa, when reducing the coefficient of thermal expansion in the embedment. The effect of reducing the coefficient of thermal expansion in the embedment on the stress component normal to the tunnel direction 0.02 m from the hole wall can be studied in Figure 5-26 through Figure 5-29.

5.4.2 Effects of overestimating the Young's modulus

In the second analysis Young's modulus was decreased from 76 GPa to 55 GPa in the embedment to study the influence on the pillar stress state. The 55 GPa value represents the rock mass modulus according to Staub *et al*., 2004. The simulation with the lower Young's modulus gives 34.4 MPa as the maximal stress component normal to the tunnel direction. The effect of reducing Young's modulus in the embedment on the stress component normal to the tunnel direction 0.02 m from the hole wall can be studied in Figure 5-26 through Figure 5-29.

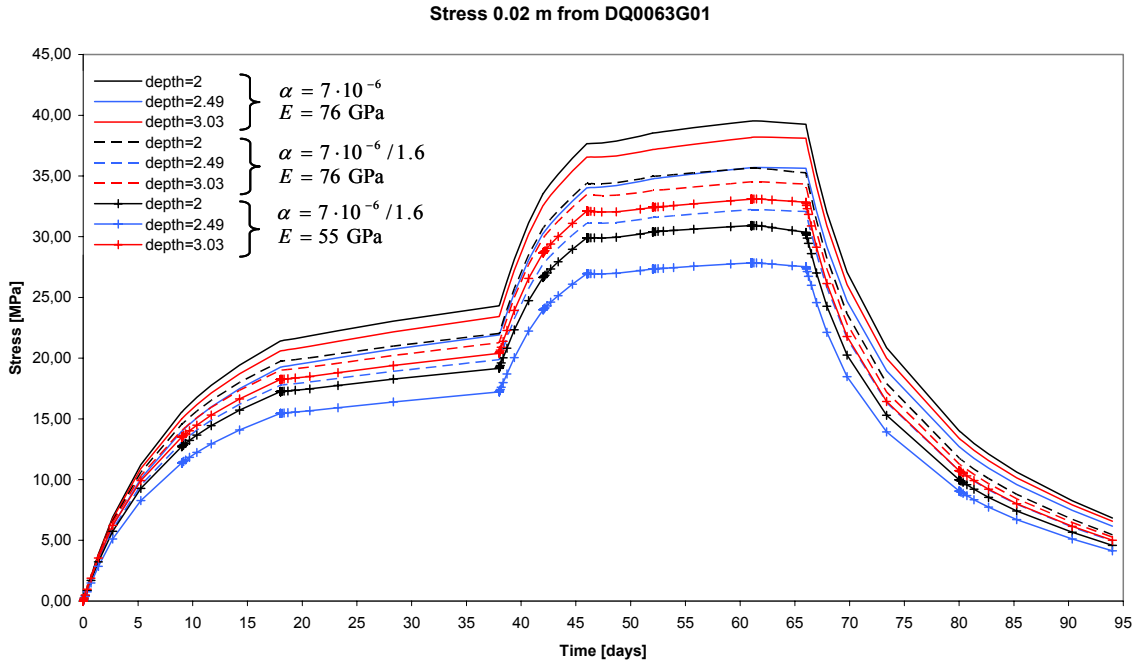

Figure 5-26. *Effects from the sensitivity analysis on the stress component normal to the tunnel direction 0.02 m from DQ0063G01. Results from upper part of the pillar. An enlarged copy of this figure is also presented in Appendix.*

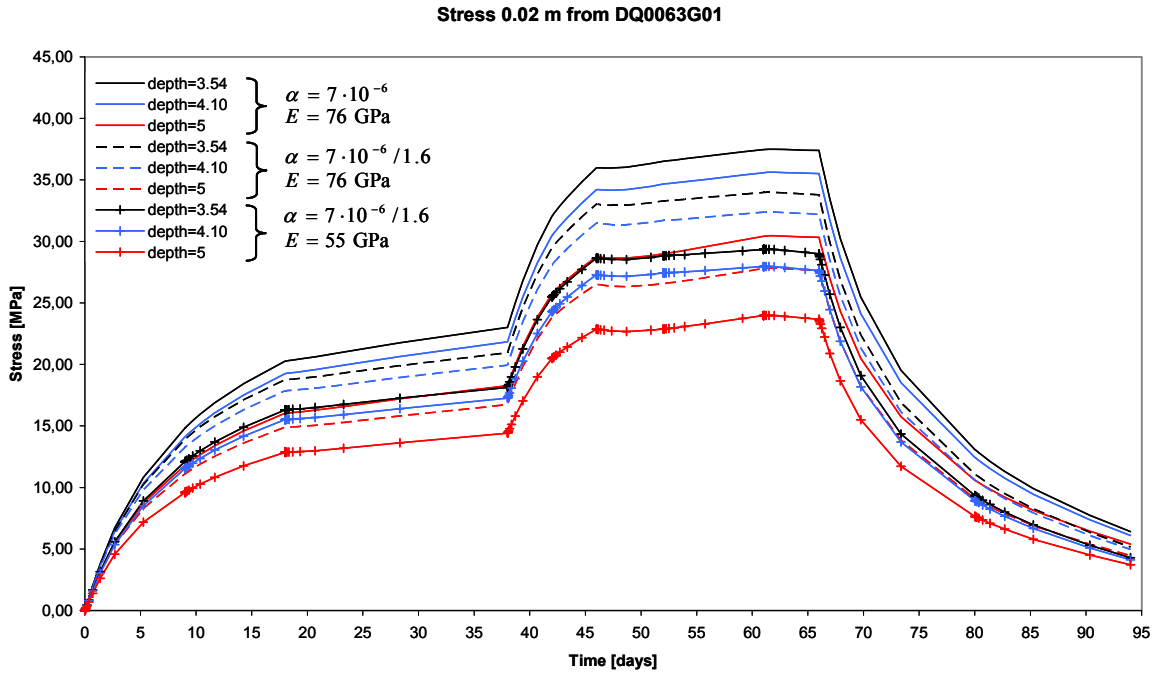

Figure 5-27. *Effects from the sensitivity analysis on the stress component normal to the tunnel direction 0.02 m from DQ0063G01. Results from lower part of the pillar. An enlarged copy of this figure is also presented in Appendix.*

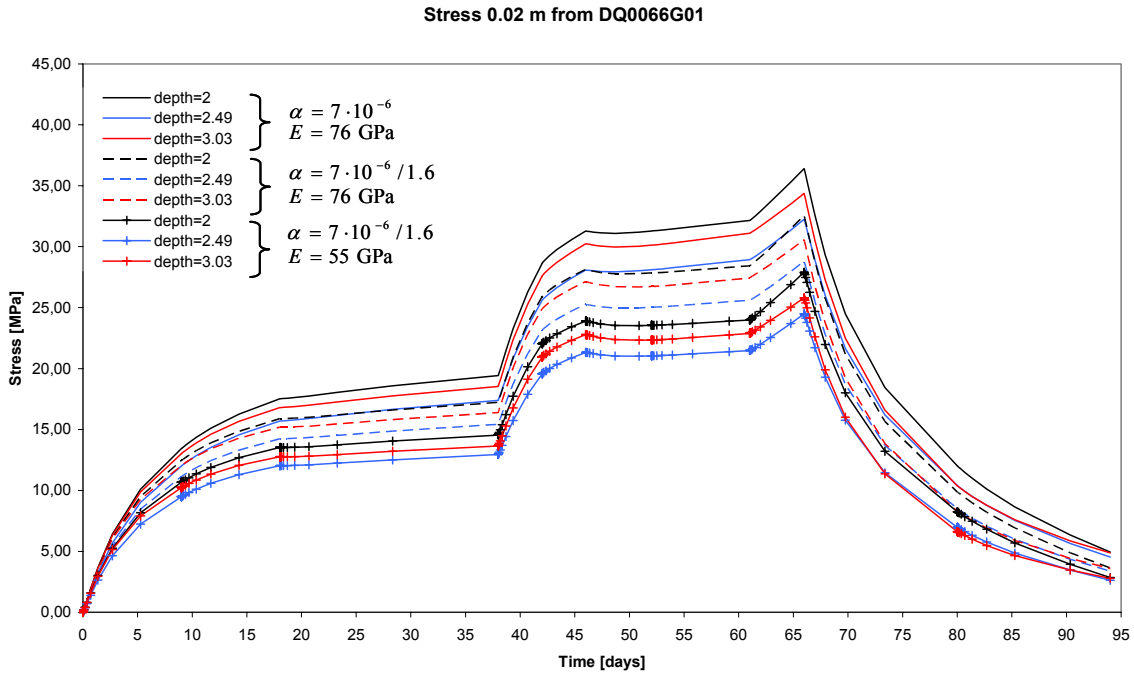

Figure 5-28. *Effects from the sensitivity analysis on the stress component normal to the tunnel direction 0.02 m from DQ0066G01. Results from upper part of the pillar. An enlarged copy of this figure is also presented in Appendix.*

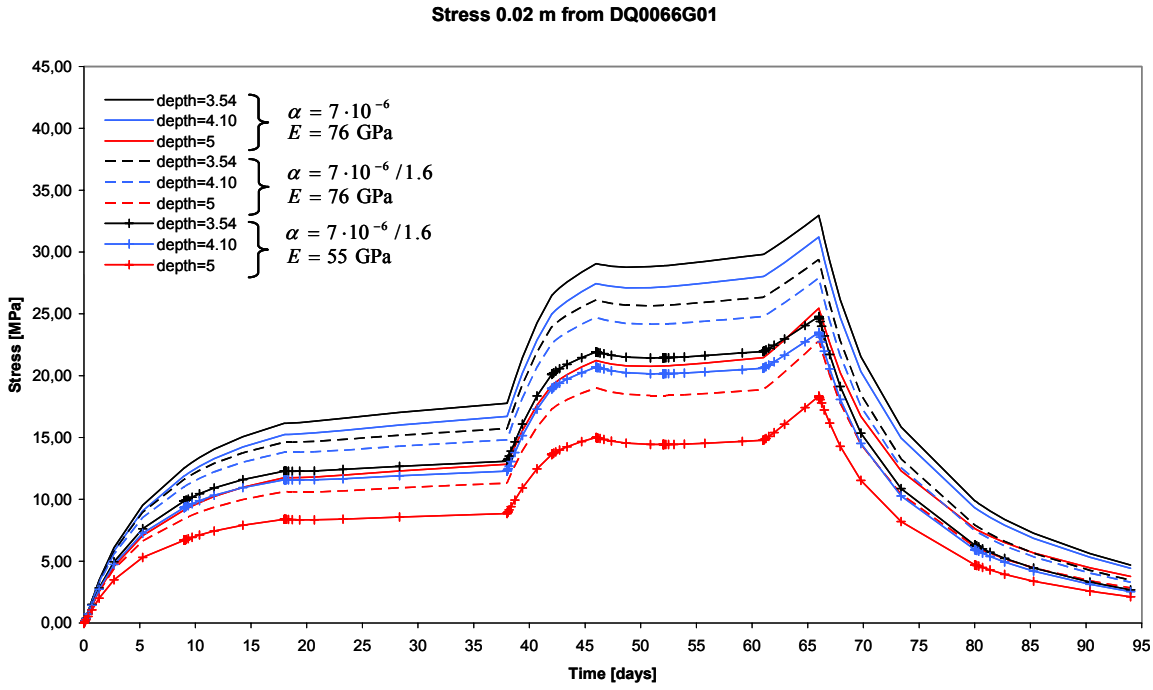

Figure 5-29. *Effects from the sensitivity analysis on the stress component normal to the tunnel direction 0.02 m from DQ0066G01. Results from lower part of the pillar. An enlarged copy of this figure is also presented in Appendix.*

6 Discussion

For points in the pillar region, recorded temperatures were reproduced in the model within a few degrees, however there were some exceptions. On the left-hand side of the experiment, the low temperature at the 3.5 m level was not captured (Figure 5-6). There were no indications of steam or extensive water movements that could explain that low temperature. It is not possible to determine if this is a true effect caused by, for instance, poor heater-rock thermal contact at a section of the two heaters, or if the measurement is not valid. The modeling was based on the assumption that the measurement was not valid.

Outside the pillar region, the calculated rock temperatures were 4 or 5 degrees higher than the measured ones. This corresponds to about 60 % overestimation of the temperature increase. The error in pillar rock stresses that would result from such a general 60 % overestimation of the temperature increase outside the immediate experiment area was estimated by analyzing a model in which the thermal volume expansion coefficient for the outer parts was reduced correspondingly. This resulted in the maximum calculated tangential stress at the tunnel/hole intersection being reduced from 43 MPa (c.f. Figure 5-13) to 38 MPa, i.e. by about 15 %. The average tangential stress reduction was about 10 %, as Figure 5-26 through Figure 5-29 shows.

The pillar rock stresses were calculated using elastic properties valid for intact rock (E=76 GPa) rather than for the rock mass (E=55 GPa). In the APSE experiment the scale of the problem is small, which means that differences between intact rock properties and rock mass properties are difficult to handle in a relevant way. The determination of the rock mass deformation modulus was based on back-calculations of the tunnel convergence observed during the excavation /Staub *et al.,* 2004/. Tunnel convergence is a process that involves large volumes of rock mass above, below and on both sides of tunnels, while the thermo-mechanical disturbance generated by the heaters in APSE did not reach more than a couple of meters from the pillar (c.f. Figure 5-13 and Figure 5-15). Therefore it may be a reasonable compromise to use intact rock properties (E = 76 GPa) for the pillar region and rock mass properties (E = 55 GPa) for the rest of the model, such as was done in the sensitivity analysis. Reducing the modulus from 76 GPa by 28 % to 55 GPa in the outer parts of the model gave, about 10 %, reduction of the maximum tangential stress. The average stress reduction was about 15 %, as Figure 5-26 - Figure 5-29 show.

The model using the lower values of thermal expansion coefficient (7×10^{-6}) and Young's modulus (55 GPa) in the outer parts of the model is believed to be the most realistic one. In this model, the tangential stress in the pillar 0.02 m from the wall of the open hole at 2 – 4 m depth, was found to be approximately 20 MPa at day 38 (before the power increase) and 30 MPa at day 52 (after the power increase) (c.f. Figure 5-26 and Figure 5-27).

References

Andersson J. C., 2003. Äspö Pillar Stability Experiment. Feasibility Study. SKB IPR-03-01

Andersson J. C., 2004. Äspö Pillar Stability Experiment. Summary of preparatory work and predictive modeling. SKB IPR-03-02

CIMNE, 2000. CODE_BRIGHT. A 3-D program for thermo-hydro-mechanical analysis in geological media. Departamento de Ingeniería del Terreno; Cartográfica y Geofísica, UPC, Barcelona, Spain.

Claesson J., 1996. Partial differential equations – Technical applications. Depts. of Mathematical and Building Physics. Lund University of Technology, Lund.

Fredriksson A., Staub I., Janson T., 2003. Äspö Pillar Stability Experiment. Design of heaters and preliminary results from coupled 2D thermo-mechanical modeling. SKB IPR-03-03

Fredriksson A., Staub I., Outters N., 2004. Äspö Pillar Stability Experiment. Final 2D coupled thermo-mechanical modeling. SKB IPR-04-02

Hökmark and Fälth, 2003. Thermal dimensioning of the deep repository. Influence of canister spacing, canister power, rock thermal properties and near field design on the maximum canister surface temperature. Technical Report TR-03-09

Rinne M., Baotang S., Lee H., 2004. Äspö Pillar Stability Experiment. Modeling of fracture development of APSE by FRACOD. SKB IPR-04-04

Staub I., Andersson J. C., Magnor B., 2004. Äspö Pillar Stability Experiment. Geology and mechanical properties of the rock in TASQ. SKB R-04-01

Wanne T., Johansson E., 2003. Äspö Pillar Stability Experiment. Coupled 3D thermo-mechanical modeling. Preliminary results. SKB IPR-03-04

Wanne T., Johansson E., Potyondy D., 2004. Äspö Pillar Stability Experiment. Final coupled 2d thermo – mechanical modeling. Preliminary particle – mechanical modeling. SKB IPR-04-03

Appendix: Copies of Figures 5-26 - 5-29.

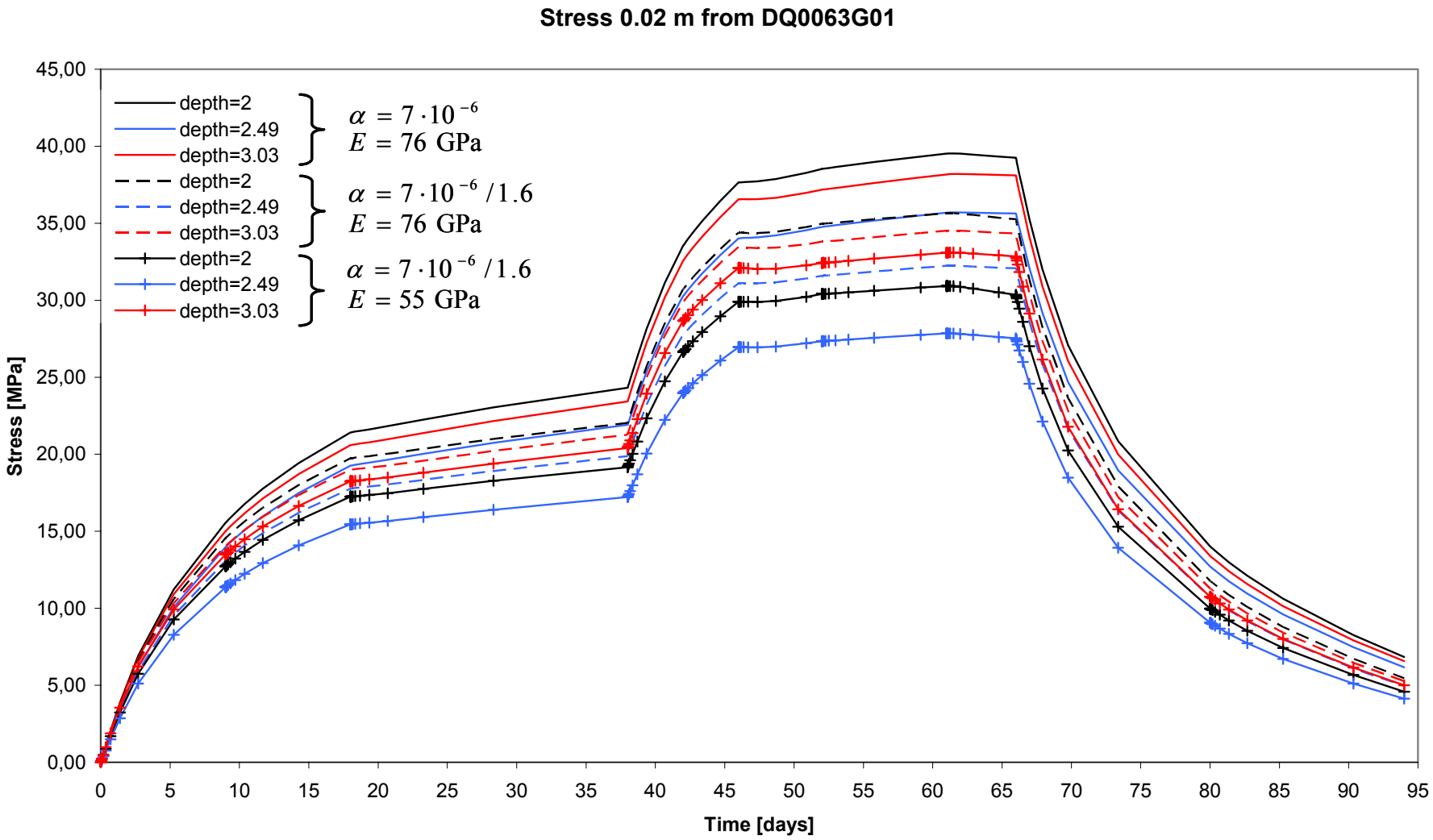

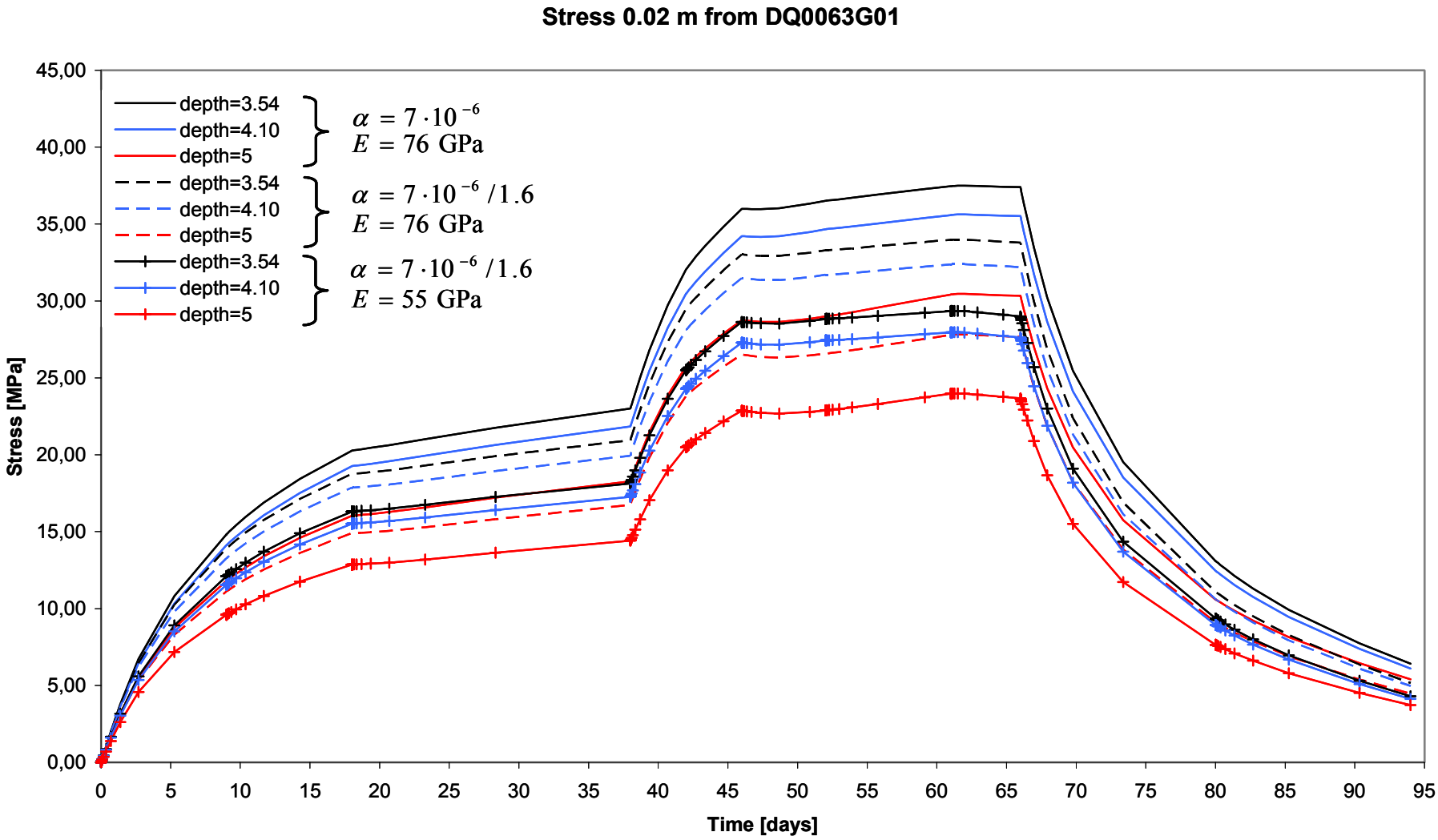
Stress 0.02 m from DQ0063G01
Stress [MPa]
Time [days]
depth=3.54
depth=4.10
depth=5
depth=3.54
depth=4.10
depth=5
depth=3.54
depth=4.10
depth=5
$\alpha = 7 \cdot 10^{-6}$
$E = 76$ GPa
$\alpha = 7 \cdot 10^{-6} / 1.6$
$E = 76$ GPa
$\alpha = 7 \cdot 10^{-6} / 1.6$
$E = 55$ GPa
45,00
40,00
35,00
30,00
25,00
20,00
15,00
10,00
5,00
0,00
0
5
10
15
20
25
30
35
40
45
50
55
60
65
70
75
80
85
90
95

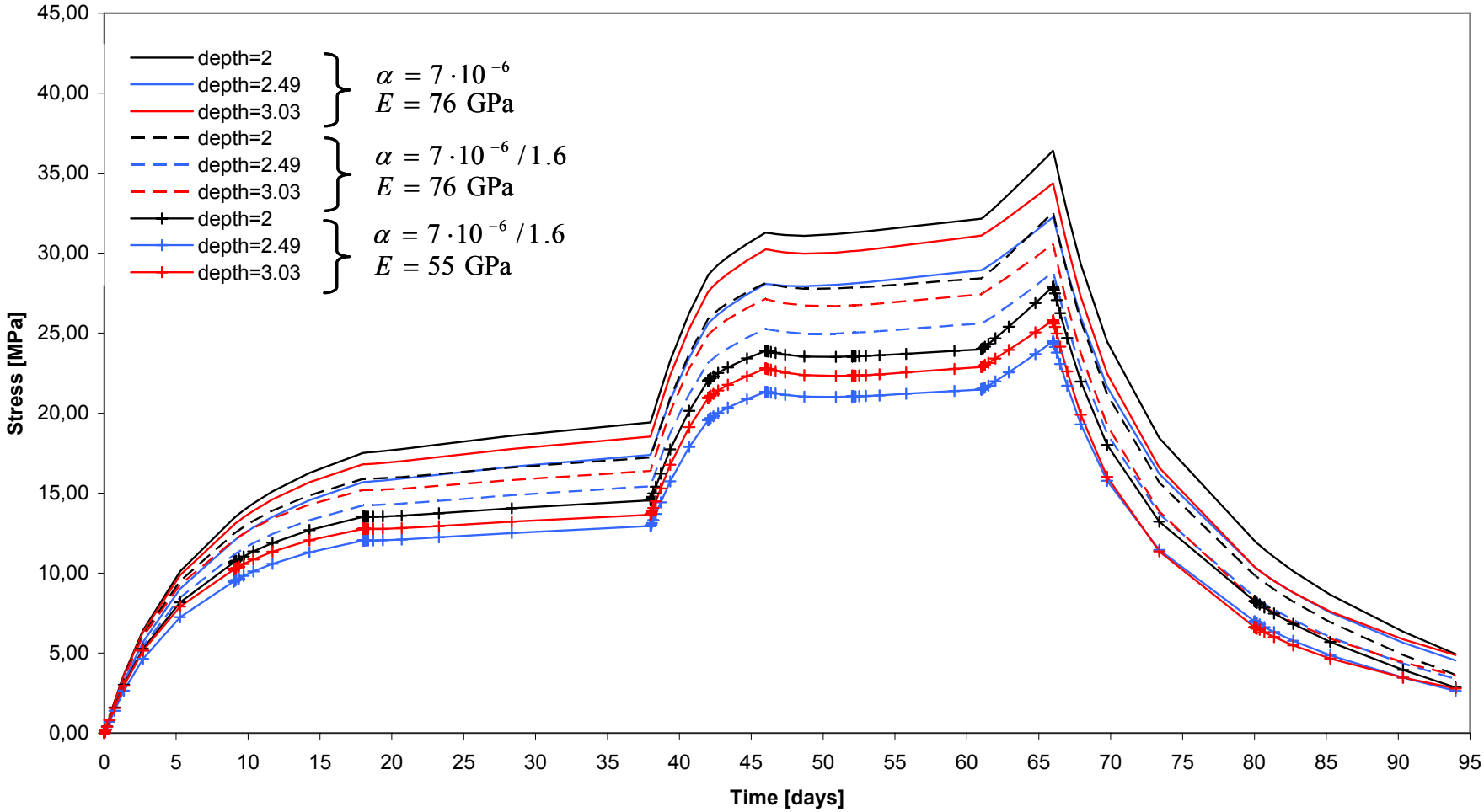
Stress 0.02 m from DQ0066G01
Stress [MPa]
Time [days]
depth=2
depth=2.49
depth=3.03
depth=2
depth=2.49
depth=3.03
depth=2
depth=2.49
depth=3.03
$\alpha = 7 \cdot 10^{-6}$
$E = 76$ GPa
$\alpha = 7 \cdot 10^{-6} / 1.6$
$E = 76$ GPa
$\alpha = 7 \cdot 10^{-6} / 1.6$
$E = 55$ GPa
45,00
40,00
35,00
30,00
25,00
20,00
15,00
10,00
5,00
0,00
0
5
10
15
20
25
30
35
40
45
50
55
60
65
70
75
80
85
90
95

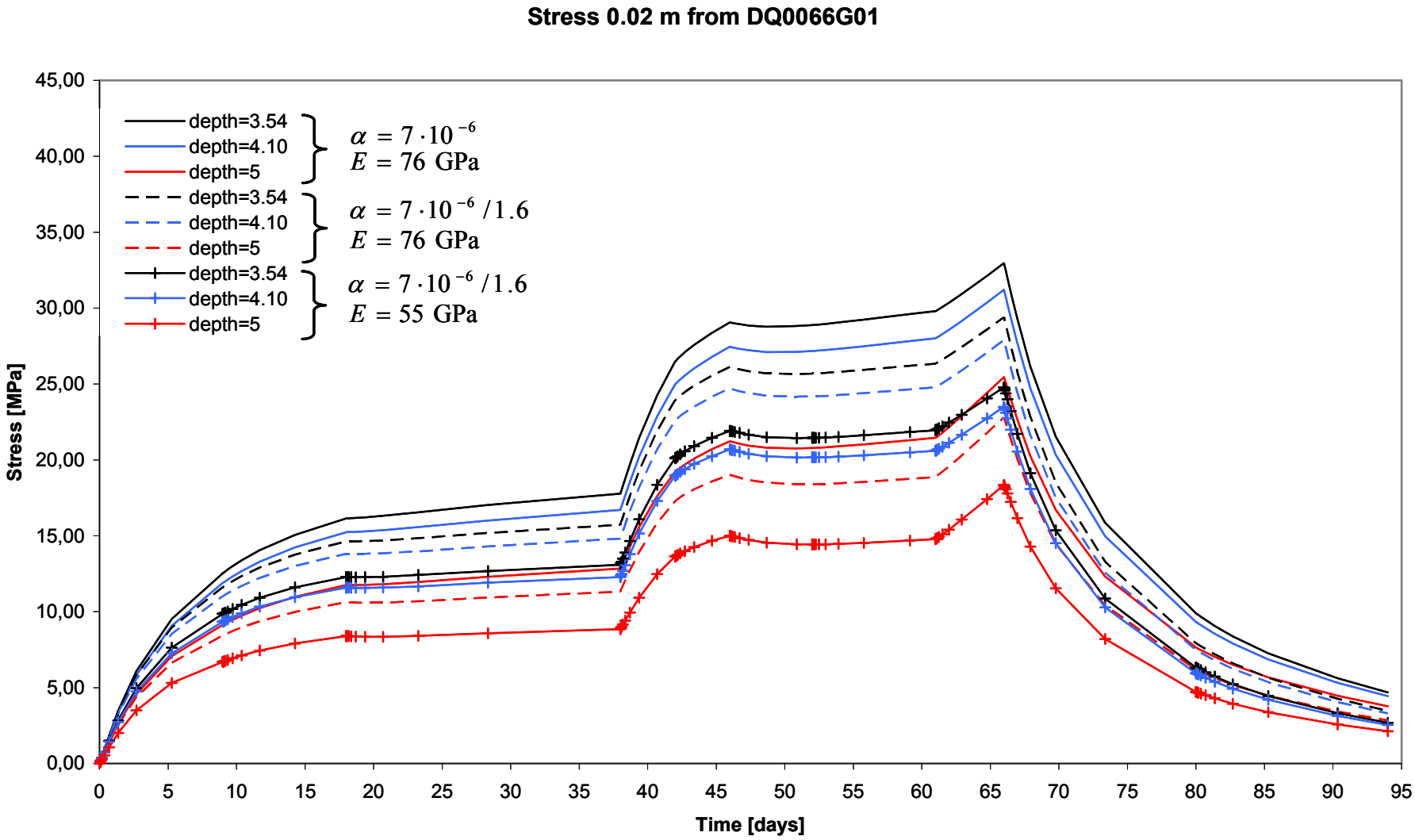
Stress 0.02 m from DQ0066G01
Stress [MPa]
Time [days]
depth=3.54
depth=4.10
depth=5
depth=3.54
depth=4.10
depth=5
depth=3.54
depth=4.10
depth=5
$\alpha = 7 \cdot 10^{-6}$
$E = 76$ GPa
$\alpha = 7 \cdot 10^{-6} / 1.6$
$E = 76$ GPa
$\alpha = 7 \cdot 10^{-6} / 1.6$
$E = 55$ GPa
45,00
40,00
35,00
30,00
25,00
20,00
15,00
10,00
5,00
0,00
0
5
10
15
20
25
30
35
40
45
50
55
60
65
70
75
80
85
90
95